algorithms

MDPI

Article

Improved Bacterial Foraging Optimization Algorithm with Machine Learning-Driven Short-Term Electricity Load Forecasting: A Case Study in Peninsular Malaysia

Farah Anishah Zaini [1], Mohamad Fani Sulaima [1,*], Intan Azmira Wan Abdul Razak [1], Mohammad Lutfi Othman [2] and Hazlie Mokhlis [3]

[1] Faculty of Electrical Technology and Engineering, Universiti Teknikal Malaysia Melaka, Durian Tunggal, Melaka 76100, Malaysia; m012210020@student.utem.edu.my (F.A.Z.); intan.azmira@utem.edu.my (I.A.W.A.R.)
[2] Advanced Lightning, Power and Energy Research (ALPER), Department of Electrical and Electronics Engineering, Faculty of Engineering, Universiti Putra Malaysia, Serdang 43400, Malaysia; lutfi@upm.edu.my
[3] Department of Electrical Engineering, Faculty of Engineering, Universiti Malaya (UM), Kuala Lumpur 50603, Malaysia; hazli@um.edu.my
* Correspondence: fani@utem.edu.my

Abstract: Accurate electricity demand forecasting is crucial for ensuring the sustainability and reliability of power systems. Least square support vector machines (LSSVM) are well suited to handle complex non-linear power load series. However, the less optimal regularization parameter and the Gaussian kernel function in the LSSVM model have contributed to flawed forecasting accuracy and random generalization ability. Thus, these parameters of LSSVM need to be chosen appropriately using intelligent optimization algorithms. This study proposes a new hybrid model based on the LSSVM optimized by the improved bacterial foraging optimization algorithm (IBFOA) for forecasting the short-term daily electricity load in Peninsular Malaysia. The IBFOA based on the sine cosine equation addresses the limitations of fixed chemotaxis constants in the original bacterial foraging optimization algorithm (BFOA), enhancing its exploration and exploitation capabilities. Finally, the load forecasting model based on LSSVM-IBFOA is constructed using mean absolute percentage error (MAPE) as the objective function. The comparative analysis demonstrates the model, achieving the highest determination coefficient (R^2) of 0.9880 and significantly reducing the average MAPE value by 28.36%, 27.72%, and 5.47% compared to the deep neural network (DNN), LSSVM, and LSSVM-BFOA, respectively. Additionally, IBFOA exhibits faster convergence times compared to BFOA, highlighting the practicality of LSSVM-IBFOA for short-term load forecasting.

Keywords: short-term load forecasting; least square support vector machine (LSSVM); improved bacterial foraging optimization algorithm (IBFOA); hybrid model; machine learning (ML)

Citation: Zaini, F.A.; Sulaima, M.F.; Razak, I.A.W.A.; Othman, M.L.; Mokhlis, H. Improved Bacterial Foraging Optimization Algorithm with Machine Learning-Driven Short-Term Electricity Load Forecasting: A Case Study in Peninsular Malaysia. *Algorithms* **2024**, *17*, 510. https://doi.org/10.3390/a17110510

Academic Editors: Van-Hai Bui, Xuan Zhou, Wencong Su and Akhtar Hussain

Received: 22 September 2024
Revised: 4 November 2024
Accepted: 5 November 2024
Published: 6 November 2024

1. Introduction

Energy is a cornerstone of sustainable development for nations worldwide. Over the past decade, there has been an increase in global energy demand. Malaysia, among the most highly developed states of the Southeast Asia region, has projected its total final energy consumption to almost double by 2050, driven by an increasing urban population and economic growth. The energy demand in Malaysia has correlated with gross domestic product (GDP) growth as the economy depends on energy-intensive industries such as manufacturing. However, the previous COVID-19 pandemic's impact disrupted the energy demand, which has lowered the GDP growth. In 2020, Malaysia's GDP experienced a significant decline of 5.54%, leading to a corresponding decrease in electricity generation (2.4%) and total final energy consumption (−0.5%), particularly within the industrial

sector compared to 2019. Therefore, the government has planned an economic recovery program to stimulate the economy, with an expected GDP growth of 3.44% per year from 2020 until 2030 [1]. The growth illustrates the increasing energy demand needed to achieve the goal.

Malaysia's energy landscape is projected to undergo a significant transformation, balancing anticipated demand growth with a resolute transition towards renewable energy (RE) and energy efficiency. The electricity utility in Peninsular Malaysia has set an ambitious target of achieving 20% RE capacity and attaining net-zero emissions by 2050. This goal will be pursued through a sustainable pathway that aims to reduce the emission intensity and halve coal generation capacity by 2035 [2]. The exponential growth and innovation in RE are actively shaping a more interconnected and environmentally sustainable global energy future. Accurate electricity forecasting serves a pivotal role in accelerating this transition, offering precise insights into future energy demand and facilitating optimized generation strategies that minimize environmental impact and maximize sustainability [3].

Based on the literature, electricity load forecasting has a different classification of forecasting depending on the time spans, such as very short-term load forecasting (VSTLF), short-term load forecasting (STLF), medium-term load forecasting (MTLF), and long-term load forecasting (LTLF) [4]. VSTL forecasts electricity demand in minutes to hours [5]. It helps manage building energy systems with features like energy storage and peak load response [6]. The STLF covers a time frame of hours to days. This helps power companies make daily decisions like spinning reserve control, optimal unit commitment, and scheduling preventive maintenance [7]. The MTLF forecasts load for periods of days to months. It is valuable for anticipating seasonal demand variations and informing critical decisions related to fuel purchases, maintenance planning, and utility assessments [8]. The LTLF extends beyond one year and reaches out to two decades. It plays a critical role in strategic planning for the power sector, guiding decisions on constructing new generation capacity and shaping the overall landscape of power supply and delivery systems [9].

Figure 1 summarizes the different forecasting horizons (VSTLF, STLF, MTLF, and LTLF) used in power system applications. Each horizon is characterized by its domain (application area), specific input data requirements, and the corresponding output metrics employed for model evaluation. The figure further categorizes load forecasting methods into three main types: traditional methods, machine learning methods, and hybrid methods. Autoregressive integrated moving average (ARIMA) and seasonal ARIMA (SARIMA), are traditional time series methods. In contrast, support vector machines (SVM) and artificial neural networks (ANN) are types of machine learning (ML). A hybrid method, combining a few individual models, can potentially enhance forecasting accuracy.

Least square support vector machines (LSSVM) have been widely used in the realm of load forecasting and have achieved good forecasting results. The optimization of LSSVM is necessary to improve the forecasting accuracy. The bacterial foraging optimization algorithm (BFOA) has achieved better results in many fields and using BFOA to find the optimal parameters of LSSVM helps to enhance the accuracy of the model. The hybridization of BFOA with back propagation neural network [10], multi-layer bidirectional LSTM [11], and ANN [12] for STLF have been found in the literature, which shows excellent performance in improving forecasting accuracy. However, this paper presents a novel approach by introducing the first application of improved BFOA hybridized with LSSVM for short-term electricity load forecasting.

Therefore, in this study, BFOA is selected to examine its suitability and performance when combined with LSSVM to forecast the load. Additionally, the bacteria's constant step size and its movement during chemotaxis are modified using a sine cosine equation to improve BFOA, and the improved BFOA (IBFOA) is proposed. Further, the IBFOA is used for LSSVM's parameters optimization. Therefore, the hybrid model for load forecasting based on LSSVM-IBFOA is established. The hybrid of LSSVM-IBFOA is applied for STLF of the electricity load in Peninsular Malaysia during the pandemic period. Consequently, the forecasting simulation illustrates the superiority of this hybrid optimization model in

comparison to three models: deep neural network (DNN), LSSVM, and LSSVM-BFOA. The main contribution of the paper is as followings:

1. Regarding Malaysia's geography and environment, the correlation between weather variables and the load consumption that influences the forecasting process is analyzed using Pearson's correlation coefficient method where the findings will influence the direction of the next generation research.
2. A novel improved bacterial foraging optimization algorithm (IBFOA) is proposed to optimize the important parameters of the LSSVM model and enhance the forecasting accuracy of the actual electricity load demand in reflecting the sustainable power market in Malaysia.
3. A full support validation accuracy measures are incorporated into the proposed model to evaluate performance of the LSSVM-IBFOA while giving such accurate load profile demand for the power network in Malaysia.

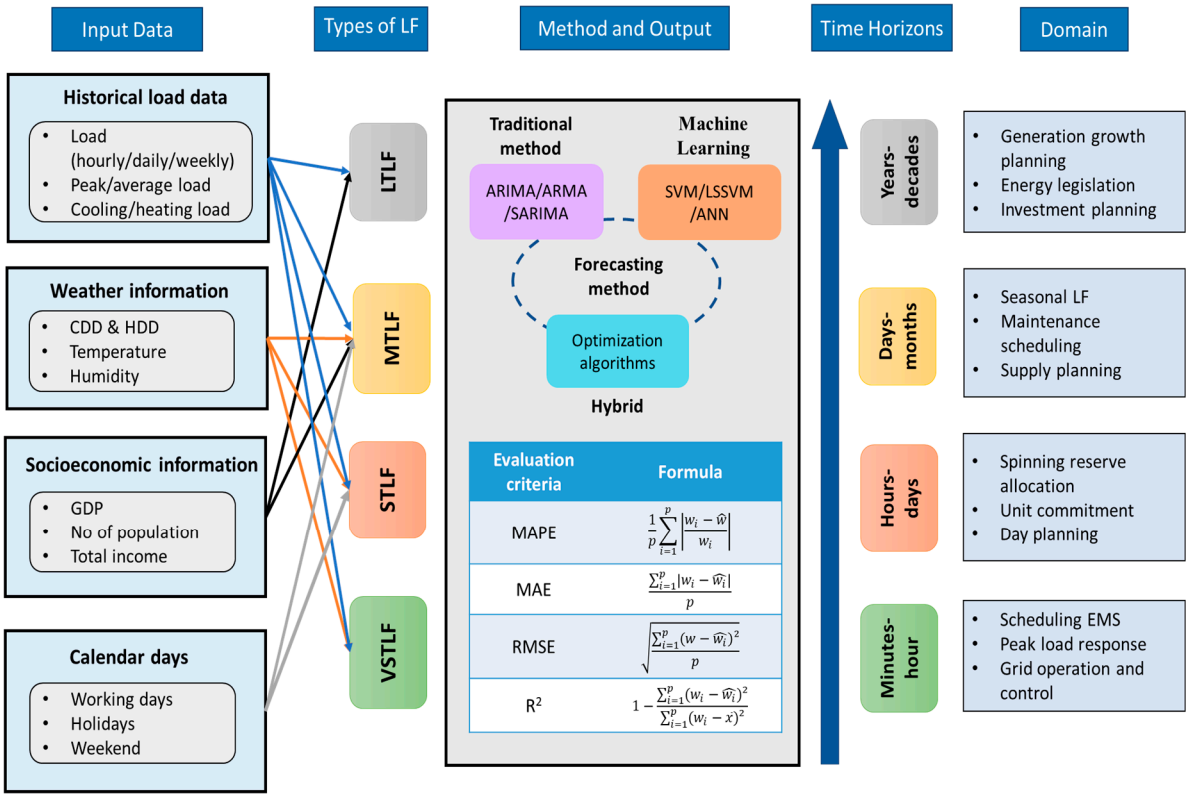

Figure 1. Summary of different types of LF with respective time horizons, domains, inputs, and outputs.

The remainder of this paper is organized as follows. Section 2 presents the previous related work. Section 3 describes the methodology used in this study. Section 4 discussed the analysis result. Finally, Section 5 gives the conclusions of the study and future recommendations.

2. Review of Related Work

STLF is inherently challenging due to the non-linear, non-stationary, and noisy nature of electricity load time series, further complicated by multiple seasonal patterns. These complexities arise from diverse electrical loads influenced by weather, calendar factors, diversity of user behavior, and penetration of renewable energy solutions [13]. Due to their direct influence on the daily electricity dispatching that powers both residents' lives and social production activities, STLF and VSTLF have emerged as the central research domains within the field of power load forecasting [14]. Additionally, STLF plays a critical

role in guaranteeing the reliability of power systems, particularly during periods of scarcity or outage. Consequently, the development of accurate STLF methodologies is essential for effective energy system planning, which in turn contributes to the improvement of the country's economic growth [15]. Hence, STLF becomes the topic of this study.

Moreover, accurately predicting electricity load necessitates careful consideration of diverse influencing factors, as demonstrated by the strong correlations observed between load demand and factors such as historical load data, calendar days, and weather patterns. In this context, STLF can be characterized as a dynamic, non-linear input and output mapping function that incorporates not only historical values but also a multitude of exogenous factors, such as weather conditions [16]. For this purpose, correlation analysis plays a pivotal role in analyzing the relationship between different factors and estimating their interdependencies. Pearson's correlation coefficient (PCC) analysis is a widely used and well-established method for this purpose [17,18]. Substantial research has employed PCC analysis to investigate the interdependency between electrical load and weather variables in load forecasting, as evidenced by studies such as [19–21]. The selection of appropriate input variables can significantly expedite model development and enhance its forecasting accuracy [22].

Different forecasting methods possess inherent strengths and weaknesses, limiting any individual method's ability to achieve consistently exceptional performance across diverse scenarios. Motivated by the need to surpass the limitations of established forecasting methodologies, the research in electricity load forecasting models has witnessed a rising trend toward hybrid models. These models integrate popular techniques with modern evolutionary algorithms and expert systems, striving to achieve high prediction accuracy and retain interpretability simultaneously [23]. The popular ML methods used in load forecasting are tree-based, neural network-based, and SVM-based methods [24].

The SVM excels in generalization; however, its computational complexity remains high due to the quadratic programming involving inequality constraints. In response, LSSVM offers an improved solution by transforming these constraints into equalities, simplifying the optimization problem [25]. This significantly reduces the computational burden, making LSSVM a more attractive choice for applications in electricity load forecasting [22,26,27]. Furthermore, the inherent influence of randomly selected internal parameters on LSSVM performance necessitates the exploration of alternative optimization algorithms to enhance its learning and generalization ability.

Evolutionary algorithms, inspired by natural selection, hold promise in identifying optimal parameter configurations for SVM, potentially leading to enhanced forecasting accuracy [28]. Among evolutionary algorithms, the BFOA garners significant recognition for its unique strengths. It excels in simultaneously exploring a vast search space (encompassing both global and local optima) and leveraging a multi-center approach [29]. The recent evolution of BFOA has improved its configuration to overcome the shortcomings of standard BFOA in terms of complexity, execution time, and convergence curve. The capability of BFOA has yielded promising results when applied to complex optimization challenges within the power system domain, such as load shedding [30,31], electric vehicle charging stations [32], frequency stabilization in hydropower systems [33], control of multi-machine power systems [34,35], economic dispatch [36], and power distribution restoration [37].

Table 1 provides a summary of the recent works of load forecasting related to hybrid SVM-based models and other recent hybrid models found in the literature. Through the summary of the literature, the hybrid forecasting model consistently exhibits superior forecasting accuracy compared to individual models. Various error metrics can be employed to evaluate the model's accuracy, including mean absolute percentage error (MAPE), mean square error (MSE), root mean square error (RMSE), cross-validation RMSE (CV-RMSE), mean absolute error (MAE) and coefficient of determination (R^2).

Table 1. Summary of related literature review for development of hybrid model in load forecasting.

Year	Hybrid Model	Main Contributions	Findings	Error Value	Application
2024	Fuzzy support vector machine-grey model (FSVM-GM) [38]	Utilized hybrid FSVM-GM for LTLF of the power system	The FSVM enhances the model's ability to fit the data and generalize to unseen data, leading to improved accuracy and reliability for LTLF	MSE = 0.6 Average error = 0.6%	Power system bus
2024	Improved variational mode decomposition—whale optimization algorithm (IVMD-WOA-LSSVM) [39]	The hybrid of IVMD-WOA-LSSVM is proposed	The WOA algorithm exhibits faster convergence and has great local optima avoidance, leading to improved optimization performance	MAPE = 3.21% CVRMSE = 0.0344 R^2 = 0.9901	Cooling load
2024	Gene expression programming—adaptive neuro fuzzy inference system (GEP-ANFIS) [40]	A hybrid of GEP-ANFIS model for LTLF is proposed and compared with single GEP and ANFIS	The proposed hybrid model consistently achieves lower error values and higher R^2 values compared to ANFIS and GEP models across all years	RMSE = 0.0007 MSE = 5.2296×10^{-7} R^2 = 0.9841 MAPE = 0.1934%	Food industry
2024	Convolutional neural network—long short-term memory (CNN-LSTM) [41]	The hybrid of CNN-LSTM is proposed and integrates with feature selection (FE) and data decomposition technique (EMD)	The EMD and FE techniques substantially enhance forecasting accuracy, leading to significant improvements in both model performance and computational complexity	MAE = 33.60 MSE = 10,599.60 RMSE = 102.95	Residential
2023	Sequential pattern mining—long short-term memory (SPM-LSTM) [42]	Hybrid of SPM-LSTM is proposed for STLF that uses load and meteorological data	SPM-LSTM outperforms LSTM, LSTM-ANN, and CNN-GA in terms of accuracy, while also requiring less training and response time	RMSE = 387.06 MAE = 207.63 CV-RMSE = 8.45% R^2 = 0.951	Cities in Spain
2022	Fuzzy cluster—fireworks algorithm—LSSVM (FC-FWA-LSSVM) [43]	Introduced a feature extraction method that combines frequency component analysis (FCA) with firefly algorithm (FA) optimization for data compression	It provides high accuracy forecasting which minimizes RMSE to 2.32%, MAPE to 2.21% compared to traditional methods	RMSE = 2.19% MAPE = 2.32% MAE = 2.40%	Residential
2022	Improved sparrow search algorithm—support vector machine (ISSA-SVM) [44]	An ISSA is proposed to address the issues with hyper parameter selection of the SVM model for mid-long term load forecasting	The ISSA-SVM can effectively improve the forecasting accuracy compared with the original SVM, BPNN, MLR, ELM, and Elman	MAPE = 2.18% Relative error = 3.94%	China's electricity consumption

3. Methodology

The model configuration follows a process illustrated in Figure 2. The data pre-processing encompassed data interpolation, Pearson correlation analysis, data division, and data normalization. The historical load data and weather data, obtained from the local website, were analyzed to assess their correlation. The load data were divided into groups based on the five-day types in the week to ensure the forecasting accuracy. The LSSVM, optimized using IBFOA, was employed for load forecasting. Finally, the proposed hybrid model is evaluated with different accuracy measures to demonstrate its performance in STLF. Further details on these processes are explained in the next subsection.

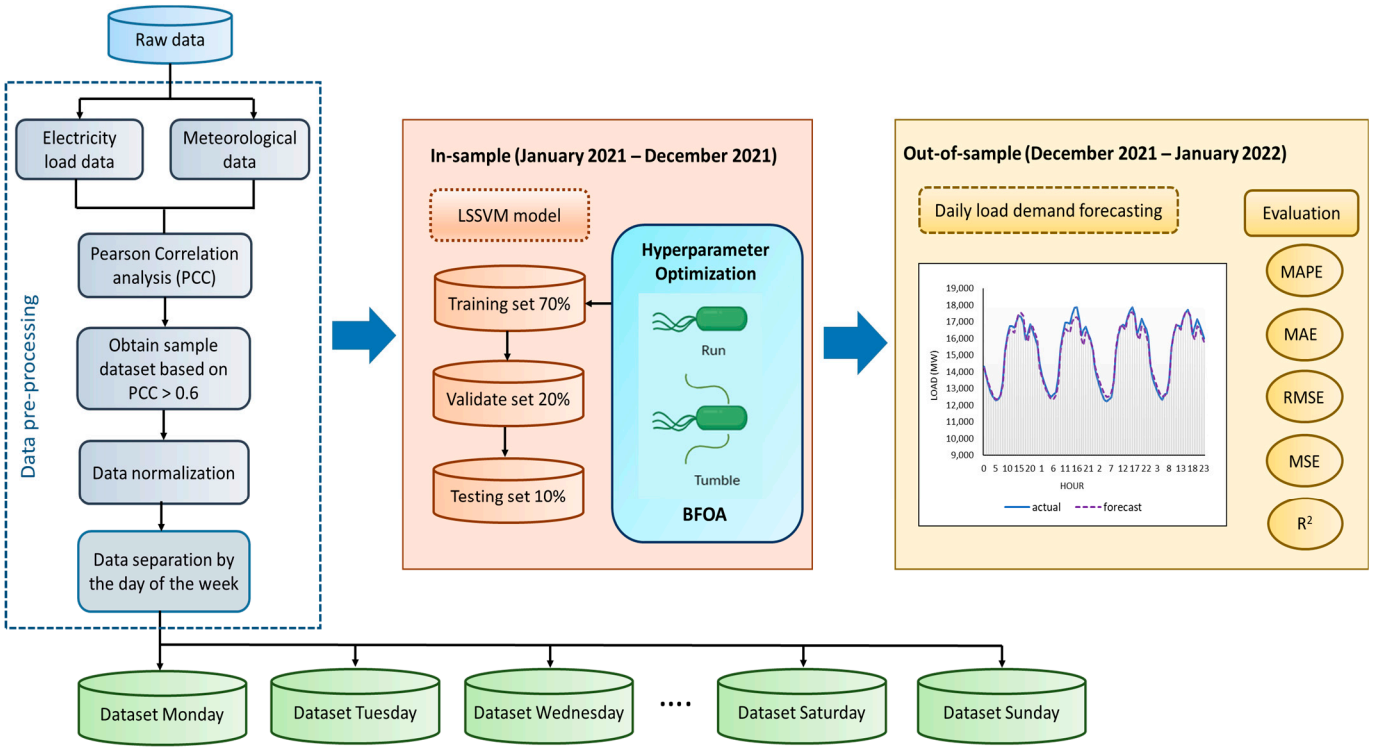

Figure 2. Framework for electricity load forecasting.

3.1. Data Pre-Processing

This section explores the data pre-processing steps and methods used to assess the correlation between electricity load and weather variables. The data division for each year is then presented in a table, illustrating the proportions allocated to training, validation, and testing before normalization is applied.

3.1.1. Data Collection

For model construction and testing, we used one confidential dataset and one publicly available dataset. The former represents electricity consumption data collected from the electricity utility of Peninsular Malaysia from year 2019 to 2021. The dataset consists of the timestamp information and electrical energy consumption in MW with frequency of 10 min every day with total sample of 1728 points. The latter represents the local weather information dataset obtained online in "Time and Date" websites consisting of hourly temperature (°C), dew point (°C), and relative humidity (%) in the same period.

3.1.2. Data Interpolation

To accurately reflect real-time behavior within the load time series, missing values were addressed through interpolation. Specifically, the "Means by Nearby Points" method was employed, guided by the following equation:

$$x' = (x_1 + x_2 + x_3 + x_4)/4 \quad (1)$$

where x_1 and x_2 denote the two preceding values, and x_3 and x_4 signify the two subsequent values (x'). This approach effectively eliminates irregularities and yields a smoother load time series.

3.1.3. Pearson Correlation Analysis

This study investigates the influence of weather variables on electricity load. The linear regression model assesses the interdependence between variables using Equation (2). In this equation, Y represents the dependent variable (electricity load), X denotes the independent variable (weather variable), "a" is the y-intercept, and "b" is the slope of the regression line.

$$y = ax + b \quad (2)$$

To further quantify the strength and direction of the linear relationship between weather variables and electricity demand, Pearson's correlation coefficient is utilized. Higher absolute values of the correlation coefficient (closer to 1) indicate a stronger, linear relationship, while values closer to 0 suggest a weaker, linear relationship. Mathematically, Pearson's correlation coefficient (r) is defined as Equation (3).

$$r = \frac{m\sum pw - \sum p \sum w}{\sqrt{\left\{n\sum x^2 - (\sum x)^2\right\}\left\{n\sum y^2 - (\sum y)^2\right\}}} \quad (3)$$

where m represents the number of data pairs, $\sum pw$ is the sum of the products of paired scores (p multiplied by w for each data point), $\sum p^2$ is the sum of squared p, and $\sum w^2$ is the sum of squared w.

The strength of the correlation between variables is interpreted based on the absolute value of the Pearson's correlation coefficient (r) as detailed in Table 2. Positive r values (0 to 1) indicate a positive correlation, while negative r values (−1 to 0) indicate a negative correlation [45,46]. This study only considers variables with strong correlations to electricity load in the model development. This approach aims to avoid the "complexity dilemma", where introducing weakly correlated variables can unnecessarily increase model complexity without improving forecasting accuracy.

Table 2. Descriptive condition based on the person correlation coefficient.

Condition	Description
$r = +1$	linear and perfect positive correlation
$0.8 < r < 1.0$	very strong linear correlation
$0.6 < r < 0.8$	strong linear correlation
$0.4 < r < 0.6$	moderate linear correlation
$0.2 < r < 0.4$	weak linear correlation
$r = 0$	no correlation exists between the two variables
$r = -1$	linear and perfect negative correlation

3.1.4. Data Division

The historical load data in 2021 were collected according to the ratio of 70% as the training set, 20% as the validation set, and 10% as the testing set. For forecasting in each day

type, only the same day type were used as historical load data for training, validation, and testing. The details of the total dataset consisting of all day types in a week are provided in Table 3.

Table 3. Forecasting dataset information.

Dataset	Period (Year 2021)	Total Days
Training set	week 1 of January–week 2 of September	252 days
Validation set	week 3 of September–week 3 of November	72 days
Testing set	week 4 of November–week 3 of December	30 days

3.1.5. Data Normalization

Data standardization is essential to ensure comparability between indicators with potentially diverse numerical ranges. This process normalizes the data by scaling them to a specific, narrower interval. In this study, a uniform mapping to the range $[-1, 1]$ was employed. Standardization offers several benefits: it accelerates model convergence and improves accuracy while also mitigating the risk of gradient explosions. Equation (4) represents the normalization method, where x represents the value to be converted, x' is the converted result, x_{max} is the maximum boundaries, and x_{min} is the minimum boundaries of the attribute values.

$$x' = 2 * \frac{x - x_{min}}{x_{max} - x_{min}} - 1 \quad (4)$$

3.2. Architecture of DNN

Table 4 outlines the architecture of the DNN model used as a comparison of ML for forecasting in this study. The model utilizes a hidden layer architecture with 100 nodes per layer, which can be adjusted based on data complexity. To stabilize the learning process, the SELU activation function was employed in the hidden layers. The Adam optimizer was selected for its efficient handling of sparse gradients and adaptive learning rate, accelerating convergence, and improving model performance [47].

Table 4. Architecture of DNN.

Parameter	Value
Number of nodes in hidden layer	100
Output shape	None, 100
Layer	1 (Dense_1)
Training algorithm	Trainim
Data division function	70/20/10
Transfer function—hidden layer	logsig
Transfer function—output layer	purelin
Activation function	Scaled exponential linear unit (Selu)
Optimizer	Adam
Epoch	100

3.3. Least Square Support Vector Machine (LSSVM)

Unlike traditional SVM, LSSVM achieves dimensionality reduction by converting the original optimization problem with inequality constraints into one with equality constraints as introduced by [48]. This transformation allows LSSVM to utilize non-linear kernel functions, effectively projecting the input data into a higher-dimensional feature space. In this study, LSSVM is leveraging to construct an error compensation model that minimizes the difference between actual and forecasted energy consumption. Let us denote the training

data as $D = \{(x_1, y_1), (x_2, y_2), \ldots, (x_n, y_n)\}$, where x_i represents the i-th input vector and y_i represents the corresponding output (actual energy consumption). The LSSVM function for this model, mapped to the high-dimensional space, can be expressed as:

$$y(x) = \omega^T \varphi(x) + b \tag{5}$$

where $\varphi(x)$ is the non-linear mapping function that projects the input vector (x_i) into a higher-dimensional space, b is the bias term that influences the overall prediction, and ω is the weight vector that determines the influence of each feature in the high-dimensional space. This transformation through the non-linear mapping function allows the LSSVM to capture complex relationships between the input variables and the output, ultimately leading to a function optimization problem that can be expressed as:

$$\min J(\omega, e) = \frac{1}{2}\|w\|^2 + \frac{1}{2}\gamma \sum_{k=1}^{N} e_k^2 \tag{6}$$

This transformation is achieved through the following equality constraint:

$$y_k = \omega^T \varphi(x_k) + b + e_k \tag{7}$$

where $\varphi(x_k)$ is non-linear mapping of the k-th input vector (projected to high-dimensional space) while e_k is a slack variable. To solve the LSSVM function optimization problem, a technique called Lagrangian transformation is employed. This method introduces Lagrange multipliers (a_k) to convert the equality constraints (Equation (7)) into an unconstrained Lagrangian function (L), defined as in Equation (8):

$$L(\omega, b, e, a) = J(\omega, e) - \sum_{k=1}^{N} a_k [\omega^T \varphi(x_k) + b + e_k - y_k] \tag{8}$$

By applying the Karush–Kuhn–Tucker (KKT) conditions as in Equation (9), the Lagrangian function is minimized to obtain the optimal values of the ω, b, e_k, and a_k. This optimization process ultimately leads to the LSSVM model for error compensation in forecasting.

$$\text{KKT} \begin{cases} \dfrac{\partial L}{\partial \omega} = 0 \rightarrow \omega = \sum\limits_{k=1}^{N} a_k \varphi(x_k) \\ \dfrac{\partial L}{\partial b} = 0 \rightarrow \sum\limits_{k=1}^{N} a_k = 0 \\ \dfrac{\partial L}{\partial e_k} = 0 \rightarrow a_k = \gamma e_k, k = 1, 2, \ldots, N \\ \dfrac{\partial L}{\partial a_k} = 0 \rightarrow \omega^T \varphi(x_k) + b + e_k - y_k, k = 1, 2, \ldots, N \end{cases} \tag{9}$$

Equation (10) is obtained after a thorough calculation as follows:

$$\begin{bmatrix} 0 & I^T \\ I & \Omega + \gamma^{-1} I \end{bmatrix} \begin{bmatrix} b \\ a \end{bmatrix} = \begin{bmatrix} 0 \\ y \end{bmatrix} \tag{10}$$

where $a = [a_1, a_2, \ldots, a_N]$, $y = [y_1, y_2, \ldots, y_N], \Omega_{ki} = \varphi(x_k)^T \varphi(x_i)$, $k, i = 1, 2, \ldots, N_o$

Due to the high dimensionality of the feature space after the non-linear mapping $\varphi(x_k)$, directly working with it can be computationally expensive. To address this, LSSVM utilizes the kernel trick. This technique leverages a kernel function $k(x, x_k)$ that operates on the original input space (x) to compute the inner product in the high-dimensional space. The Mercer condition ensures that such a kernel function exists. Mathematically, this relationship is expressed as in Equation (11) and the final regression function of LSSVM is obtained in Equation (12).

$$k(x_k, x_i) = \varphi(x_k)^T \varphi(x_i) \tag{11}$$

$$y(x) = \sum_{k=1}^{N} a_k k(x, x_k) + b \tag{12}$$

Within the LSSVM framework for this study, the radial basis function (RBF) kernel is chosen due to its well-established generalization ability and wide convergence domain. The RBF kernel function is defined as Equation (13):

$$K(x_k, x_i) = \exp(-\frac{\|x_k - x_i\|^2}{2\sigma^2}) \tag{13}$$

where σ (sigma) represents the width of the kernel function. Optimizing the parameters of the RBF kernel, particularly sigma (σ) and gamma (γ), is crucial for achieving optimal performance in the LSSVM model. These parameters significantly influence the model's ability to learn from the training data and generalize well to unseen data [49]. Therefore, after obtaining the ideal of these two values, the next stage is to optimize them using IBFOA. The structure of the LSSVM model can be visualized as depicted in Figure 3. In this structure, the final output is a linear combination of the values from intermediate nodes. Notably, each intermediate node corresponds to a support vector within the LSSVM model [50].

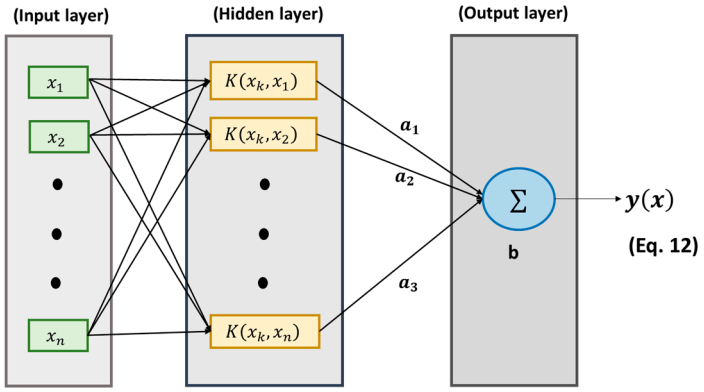

Figure 3. Structures of LSSVM.

3.4. Bacterial Foraging Optimization Algorithm

The bacterial foraging optimization algorithm (BFOA) is a population-based stochastic optimization technique inspired by the foraging behavior of *Escherichia coli* (*E. coli*) bacteria introduced by Kevin M. Passino in 2002 [51].

Assume that the population of bacteria has S numbers, and that the present chemotactic, reproductive, and elimination-dispersal steps are represented by t, r, and e, respectively. At the t-th chemotactic step, r-th reproduction, and e-th elimination dispersal, the n-th bacterium's location in the D-dimensional search space can be represented as follows:

$$\theta^n(t, r, e) = \left\{\theta_n^1(t, r, e) + \theta_n^2(t, r, e), \ldots\ldots, \theta_n^D(t, r, e)\right\} \tag{14}$$

The prominent processes take place in BFOA consisting of chemotaxis, swarming, reproduction, and elimination-dispersal are described briefly below:

- Chemotaxis: It is a process by which bacteria navigate their environment in response to chemical gradients. This behavior allows them to locate favorable conditions, such as nutrient sources. Bacteria achieve chemotaxis through a series of short runs (swims) and tumbles. Flagellar rotation determines their movement: swimming in a defined direction or tumbling to explore new areas. A unit-length random direction vector as described in Equation (15) representing a tumble for the n-th bacterium at the t-th chemotactic step, r-th reproductive step, and e-th elimination dispersal step. This vector describes the direction change after a tumble.

$$\varphi(j) = \frac{\Delta_i(t,r,e)}{\sqrt{\Delta_i^T(t,r,e)\Delta_i(t,r,l)}} \tag{15}$$

$$\theta^n(t+1,r,e) = \theta^n(t,r,e) + C(i)\varphi(j) \tag{16}$$

where $\theta^n(t+1,r,e)$ represents the n-th bacterium at the t-th chemotactic step, r-th reproductive and e-th elimination dispersal step. $C(i)$ is the size of the step taken in the random direction specified by the tumble (the run length unit) and $\Delta_n(t,r,e)$ denotes a random direction vector that describes the movement direction of the n-th bacterium.

Swarming: Swarming is a collective behavior in bacteria that promotes their movement towards areas with higher nutrient concentrations. This phenomenon is modeled by introducing an additional cost function term (J_{cc}) that influences the overall cost function (J) experienced by each bacterium. The swarming cost (J_{cc}) considers both the local bacterial density and the distance between individual bacteria.

The mathematical representation of the swarming process is expressed by Equation (17):

$$\begin{aligned} J_{cc}(\theta, P(t,r,e)) &= \sum_{n=1}^{s} j_{cc}^n(\theta, \theta^n(t,r,e)) \\ &= \sum_{n=1}^{s}\left[-d_{attract}\exp\left(-\omega_{attract}\sum_{n=1}^{m}(\theta_n - \theta^n)^2\right)\right] \\ &\quad + \sum_{n=1}^{s}\left[h_{repellant}\exp\left(-\omega_{repellant}\sum_{n=1}^{m}(\theta_n - \theta^n)^2\right)\right] \end{aligned} \tag{17}$$

The coefficients associated ($d_{attract}$, $\omega_{attract}$, $h_{repellant}$, and $\omega_{repellant}$) influence the relative importance of swarming compared to the original cost function (J). These coefficients need to be carefully chosen or tuned to achieve optimal performance in the BFOA.

- Reproduction: The reproduction step happens following a predefined number of chem otactic steps (Nc). This step promotes the propagation of "fitter" bacteria within the population. Bacteria with higher health values, typically determined by a fitness function have a greater chance of reproducing. Conversely, bacteria with lower health values will be eliminated. This mechanism ensures a constant population size while favoring individuals with better foraging abilities. The health value of the bacterium obtained as below:

$$J_{health}^i = \sum_{t=1}^{Nc} J(n,t,r,e) \tag{18}$$

- Elimination-dispersal: Elimination-dispersal simulates the dynamic nature of the bacterial environment, where local events can drastically affect bacterial populations. This process can either eliminate all bacteria in a local region or disperse them to new locations, potentially disrupting chemotaxis progress but also aiding in exploration by placing bacteria near potential food sources.

3.5. Proposed Improved Bacterial Foraging Optimization Algorithm

Like many other metaheuristic algorithms, the BFOA exhibits certain limitations, including high computational cost, inherent complexity, and susceptibility to becoming trapped in local optima [29]. These shortcomings necessitate further research efforts to enhance the performance of BFOA and address these deficiencies. The improvement of BFOA in the existing literature mainly focuses on the chemotaxis of bacteria, as shown in [52–54]. Chemotaxis, the core operation of the BFOA, relies heavily on the "chemotaxis step length" parameter $C(i)$ for effective exploration. However, the classical BFOA employs a fixed value for $C(i)$, leading to potential drawbacks. A large constant step size might hinder bacteria from reaching distant nutrient sources, while a small value could significantly slow their movement towards nearby nutrients [55].

This study introduces an improved bacterial foraging optimization algorithm (IBFOA) that modifies the chemotaxis operation using the sine cosine algorithm (SCA) for inspiration. The key improvement lies in adapting the constant step size ($C(i)$) of bacteria during chemotaxis. The standard BFOA employs a fixed step size for bacterial movement during chemotaxis. The IBFOA proposes an adaptive step size defined by Equation (19):

$$C(i) = a - t\frac{a}{S} \tag{19}$$

where a is a defined constant, and t is a count of the chemotaxis. This adaptation introduces a gradual increase in the step size as the chemotaxis process progresses. Additionally, the IBFOA incorporates a mechanism inspired by the SCA to generate random movement directions for the bacteria during chemotaxis. Equation (20) adopted from SCA generates a random direction vector for each bacterium's movement:

$$\Delta_n^d(t,r,e) = \begin{cases} \sin(r_2) \times \left| r_3 P^d(t,r,e) - X_n^d(t,r,e) \right| & r_4 < 0.5 \\ \cos(r_2) \times \left| r_3 P^d(t,r,e) - X_n^d(t,r,e) \right| & r_4 \geq 0.5 \end{cases} \tag{20}$$

where $X_n^d(t,r,e)$ and $P^d(t,r,e)$ are the current position of the n-th bacterium and the best solution so far at the t-th chemotactic step, r-th reproduction, and e-th elimination dispersal in the d-th dimension, respectively. Variables of r_2, r_3, and r_4 are a random number in between 0 and 2π, and $|\ |$ indicates the absolute value similar to SCA. The position of the n-th bacterium after a tumble is given by Equation (21):

$$\theta^n(t+1,r,e) = \theta^n(t,r,e) + \left(a - t\frac{a}{S}\right)\left(\frac{\Delta_n(t,r,e)}{\sqrt{\Delta_n^T(t,r,e)\Delta_n(t,r,e)}}\right) \tag{21}$$

If the bacterium encounters a higher nutrient concentration after a tumble (Equation (22)), it continues swimming in the same direction for a predefined number of swim lengths as long as the concentration increases. Conversely, if the concentration decreases, the bacterium performs another tumble to explore a new direction (Equations (19) and (20)). The remainder of the IBFOA follows the standard BFOA process, including reproduction and elimination-dispersal. This improved algorithm aims to achieve better exploration and exploitation capabilities compared to the original BFOA.

$$\theta^n(t+1,r,e) = \theta^n(t+1,r,e) + \left(a - t\frac{a}{S}\right)\left(\frac{\Delta_i(t,r,e)}{\sqrt{\Delta_i^T(t,r,e)\Delta_i(t,r,e)}}\right) \tag{22}$$

3.6. Forecasting Process by Hybrid LSSVM-IBFOA

Figure 4 illustrates the formation of a hybrid model of LSSVM-IBFOA where IBFOA will optimize the parameters of LSSVM to achieve accurate forecasting. The data preprocessing is performed through data separation and normalization of the load profile in Peninsular Malaysia. The LSSVM and IBFOA are merged to perform as a hybrid model and will be built separately according to day type for better forecasting performance. The optimization process is initiated with random positions for each bacterium in the predefined dimensions, which represent the LSSVM parameters. The optimized LSSVM parameters are used to train the LSSVM. The trained model is tested on unseen data. The objective function, MAPE, is observed. The modification of IBFOA parameters is performed to optimize the LSSVM parameters, which in turn produces an accurate forecast or lowest MAPE. Table 5 provides the formation step of hybrid LSSVM-IBFOA accordingly.

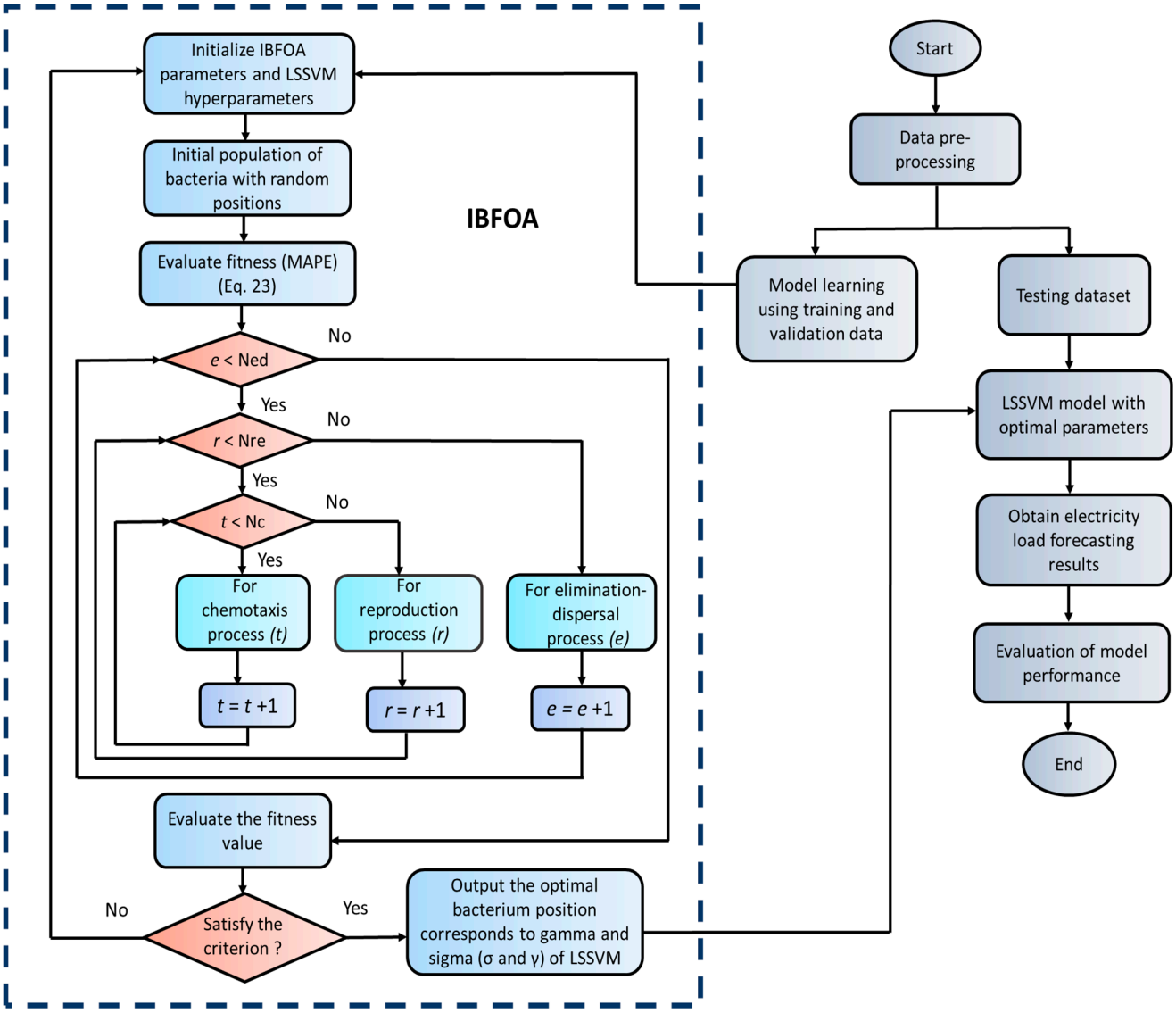

Figure 4. The flowchart of LSSVM-IBFOA.

Table 5. Formation step of hybrid LSSVM-IBFOA.

Number of Steps	Description
Step 1	Collecting the historical power load data for the analysis and stored in a MATLAB file format (.mat). The load function in MATLAB is then employed to import these data into the workspace
Step 2	The power load forecasting dataset is divided into training data, validation data and testing data according to the ratio 70:20:10, and the data are normalized
Step 3	Parameters setting: p, n, S, Nc, Ns, Nre, Ned, Ped where p is the number of parameters to be optimized, S is the number of bacteria, Ns is the swimming length, Nc is the maximum number of iterations in chemotaxis, Nre is the maximum number of reproduction, Ned is the maximum number of elimination dispersal, Ped is the probability of elimination-dispersal

Table 5. *Cont.*

Number of Steps	Description
Step 4	Generate the initial population of bacteria with random positions
Step 5	Create an initial population of bacteria with random positions where each bacterium's positions encode the LSSVM parameters
Step 6	Set the fitness function
Step 7	For each bacterium, train an LSSVM model with the corresponding parameters on historical load data. Evaluate the fitness of each bacterium based on the mean absolute percentage error (MAPE) value: $\text{Fitness} = \text{MAPE} = \frac{1}{p}\sum_{i=1}^{p}\left\lvert\frac{w_i-\hat{w}}{w_i}\right\rvert$ (23) where p is the total number of forecasting data, w_i is the actual value and $\hat{w}_i$ is the forecasted value
Step 8	Elimination-dispersal: $e = e + 1$
Step 9	Reproduction loop: $r = r + 1$
Step 10	Chemotaxis loop: $t = t + 1$
Step 11	Update the positions of bacteria based on BFOA's chemotaxis mechanism (Equation (20))
Step 12	Go to step 8 if $t <$ Nc
Step 13	Perform reproduction
Step 14	Select bacteria for reproduction based on their fitness value
Step 15	Go to step 7 if $r <$ Nre
Step 16	Perform elimination-dispersal
Step 17	Eliminate and disperse each bacterium with probability of Ped. Go to step 6 if $e <$ Ned
Step 18	Evaluate fitness and selection
Step 19	Train LSSVM models using the updated positions of bacteria. Evaluate the fitness of the updated bacteria by using Equation (23)
Step 20	Use the LSSVM-IBFOA to forecast the test data and select MAPE as the objective function for forecasting $\text{Fobj} = \text{MAPE} = \frac{1}{p}\sum_{i=1}^{p}\left\lvert\frac{w_i-\hat{w}}{w_i}\right\rvert$ (24)
Step 21	Inverse normalize the forecasting results
Step 22	Output the accuracy measures for evaluation

3.7. Evaluation Metrics

Evaluating the accuracy of the forecasting model is crucial for assessing the effectiveness of the proposed methods. This section discusses the key performance criteria used in this study. The mean absolute error (MAE) and mean absolute percentage error (MAPE) are the most important static metrics used by researchers [56]. In the simulation, MAPE is utilized as an objective function of LSSVM-IBFOA (fitness function value). It is a widely adopted performance measure in the electric power industry due to its simplicity and ease of interpretation [57]. The MAPE value was classified into four forecasting capabilities, as provided in Table 6 for business and industrial data as reviewed in [58]. This table was also referred in [59,60] for annual power load forecasting at regional and national levels considering LTLF.

Table 6. Forecasting capability based on the MAPE value.

MAPE (%)	Forecasting Capability
<10	Highly accurate forecasting
10–20	Good forecasting
20–50	Reasonable forecasting
>50	Inaccurate forecasting

A thorough assessment of the model's performance requires employing a diverse set of accuracy measures. This section details the metrics used in this study along with their interpretations. These accuracy measures include MAE, MSE, RMSE, R2, NRMSE, and NMSE, which are obtained by equations in Table 7, where p is the total number of forecasting data, w_i is the actual value, $\hat{w}_i$ is the forecasted value and $\overline{x}$ is the average value of forecasted value [61]. The best state to evaluate the accuracy of forecasting results using such measures is the maximum value for R2 and the minimum value for forecasting error measures [62]. The simulation of LSSVM models is done using MATLAB language version R2022b and the DNN model using Python language. All development and experimental works were carried out on a personal computer with processor Intel(R) Core(TM) i7-4790 @ 3.60 Ghz with 16 GB of RAM.

Table 7. Descriptive of accuracy measures for performance evaluation.

Measures	Criteria	Description	Equation	No. of Equation
MAPE	Mean absolute percentage error	Reflects the degree of data dispersion and accurately captures the actual forecasted data [63]	$\frac{1}{p}\sum_{i=1}^{p}\left\|\frac{w_i-\hat{w}}{w_i}\right\|$	(25)
MAE	Mean absolute error	Shows the mean distance between the actual and forecasted values	$\frac{\sum_{i=1}^{p}\|w_i-\hat{w}_i\|}{p}$	(26)
MSE	Mean square error	Reflects the degree of dispersion of the dataset [63]	$\frac{\sum_{i=1}^{p}(w_i-\hat{w}_i)^2}{p}$	(27)
RMSE	Root mean square error	Captures the average error between the forecasted value and the actual value [63]	$\sqrt{\frac{\sum_{i=1}^{p}(w-\hat{w}_i)^2}{p}}$	(28)
R^2	Determination coefficient	Determines the proportion of the variance in the dependent variable that is predictable from the independent variables [64]	$1-\frac{\sum_{i=1}^{p}(w_i-\hat{w}_i)^2}{\sum_{i=1}^{p}(w_i-\overline{x})^2}$	(29)
NRMSE	Normalized root mean square error	Normalizes the RMSE by dividing it by the average of the actual values. Prone to the influence of large outliers [65]	$\frac{\sqrt{\frac{\sum_{i=1}^{p}(w_i-\hat{w}_i)^2}{p}}}{\frac{1}{p}\sum_{i=1}^{p}w_i}$	(30)

4. Results and Discussion

4.1. Correlation Analysis

In this analysis, some of the weather variables considered include relative humidity, dew point, and temperature. Relative humidity signifies the ratio of water vapor present in the air compared to the maximum amount it can hold at that temperature, expressed as a percentage. Higher humidity during warmer months amplifies the sensation of heat compared to the actual temperature [17]. These weather variables are often included together due to their inherent interdependencies.

Table 8 presents the correlation coefficient between the load consumption and the model inputs. The correlation coefficients were computed for load and weather variables

over a 48-day period. Notably, the previous day's load exhibits a strong positive correlation with the current day's load, indicating a significant influence on the forecasted load. The relative humidity and temperature show a moderate correlation, while the dew point shows weak and no correlation with load because the correlation coefficients are less than ± 0.6, as mentioned in Table 2. Thus, the simulation model only considered the input from the previous load with a strong correlation whereas weather variables are neglected.

Table 8. Correlation coefficients between the load and the model inputs (variables).

No	Variables	Pearson Correlation Coefficient (*r*), (load and Model Inputs)
1	Last day relative humidity (%)	−0.4351
2	Last two days' relative humidity (%)	−0.4965
3	Last week relative humidity (%)	−0.5302
4	Last day temperature (°C)	0.4874
5	Last two days' temperature (°C)	0.5653
6	Last week temperature (°C)	0.5676
7	Last day dew point (°C)	−0.0945
8	Last two days' dew point (°C)	−0.2429
9	Last week's dew point (°C)	−0.0421
10	Last day load (MW)	0.7762
11	Last two days' load (MW)	0.7256
12	Last week load (MW)	0.6457

4.2. Case Study

In this study, the electricity load of Peninsular Malaysia during the COVID-19 pandemic was used as a case study for evaluating the efficiency of the proposed model in disrupted situations. The hourly electricity load demand in megawatts (MW) in 2021 was used as raw input data. Figure 5 depicts the monthly average electricity load demand in 24 h, illustrating the characteristics of the electricity load pattern. During the year of pandemic (2020 and 2021), the electricity load fluctuated and did not follow the trend of the pre-pandemic (2019). For instance, in March 2020, the electricity load dropped by 23.54% compared to the same month in 2019. This is due to the enforcement of the initial movement control order (MCO) 1.0 on 18 March which closed non-essential business operations and restricted human daily activities to control the spread of the virus. The MCO 2.0 was enforced in the early months of 2021 but failed to achieve a significant reduction in COVID-19 cases as it was only enforced in certain states. Therefore, the full nationwide lockdown (MCO 3.0) was implemented in June 2021 due to the rise in COVID-19 cases. Consequently, the average electricity consumption in June 2021 was 1109 MW lower than the average consumption for the same month in 2019, which represents a reduction of 7.69%. From October 2021, a recovery in the load demand can be seen with the further easing of some restrictions and allowing some activities to continue.

The COVID-19 pandemic is considered a crisis event due to the unprecedented measures implemented and the demand pattern during the pandemic is expected to be different than the previous periods. Thus, electricity demand needs to be forecasted considering the fluctuating demand pattern. Although the impact of the pandemic is obvious, accurate forecasting remains essential for effective market operations and system planning [66]. Therefore, in this paper, the load demand from January until December 2021 is taken as the case study to observe the ability of the LSSVM-based model to forecast the future load patterns based on past load behavior during the pandemic.

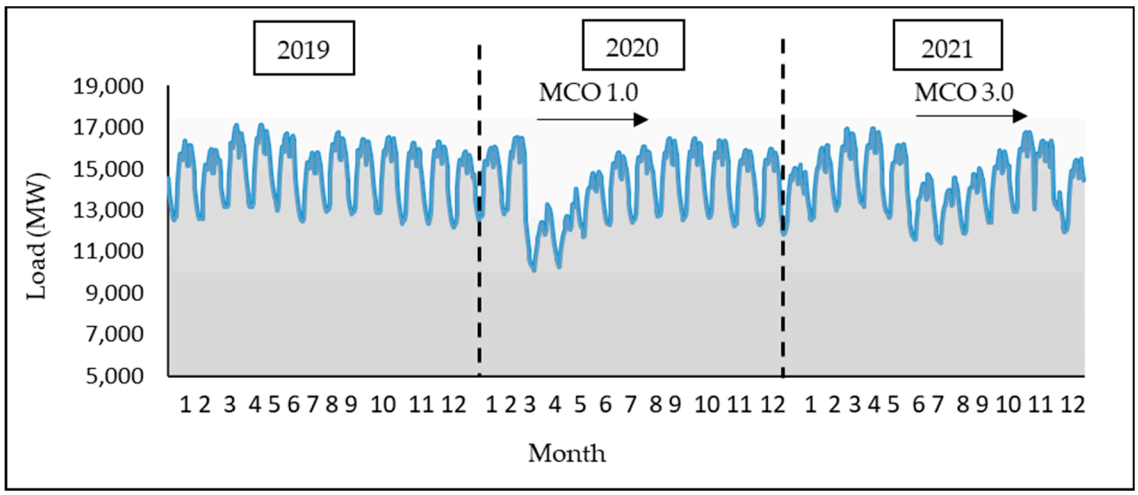

Figure 5. Monthly average electricity load profile in 24 h (2019–2021).

Seasonality in Load

To capture daily and weekly seasonal patterns, a common approach involves decomposing load data into different day types, each exhibiting a unique load profile. Previous research has established the existence of multiple day types, which are typically identified through a combination of forecaster expertise and clustering methodologies. Typical similar day-based STLF methods predict the load of a target day by leveraging the load profile of a historically similar day, complemented by relevant external factors [67]. Classifying the historical load data by the day of the week will aid in improving the accuracy of STLF since the loads on weekdays are probably higher than on weekends [68]. Some scholars used to label the days to be forecasted differently based on the day-type characteristics [69–71]. The model described in the next section is of this kind. The typical weekly load profile in December 2021 for Peninsular Malaysia is depicted in Figure 6. The first day of the week (Monday) and weekend (Saturday and Sunday) exhibit different load profile curves compared to other days.

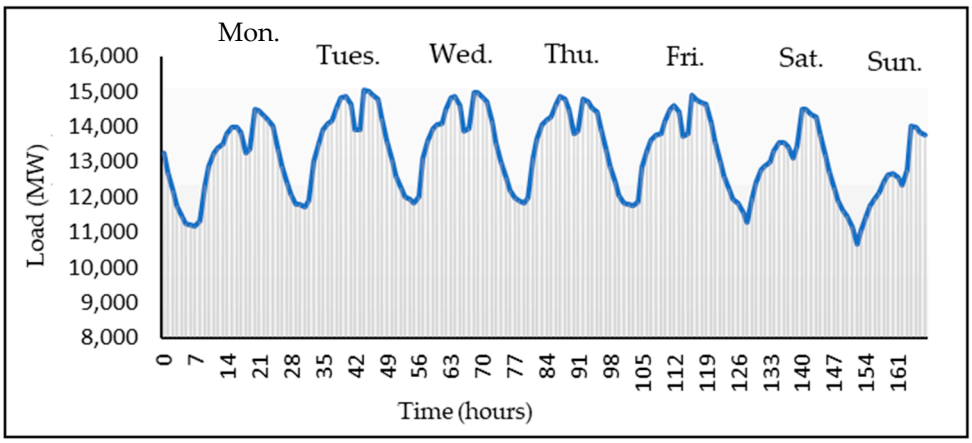

Figure 6. Typical weekly average load profile in December 2021.

For yearly seasonality, some researchers [72,73] selected the same day type in the same season (summer, winter, autumn, and spring) of different months throughout the year. The load consumption in summer and winter is usually higher than in other season due to the increasing use of cooling and heating appliances in these seasons [74]. The author of [75,76] introduced different forecasting model for periods of the year, especially during holidays such as public holidays, Easter Day, Christmas, and New Year's Day.

4.3. Load Forecasting Results

The following section presents an analysis of the performance of LSSVM in conjunction with BFOA and IBFOA based on different evaluation criteria, as listed in Table 5. In this paper, four models, namely DNN, LSSVM, LSSVM-BFOA, and LSSVM-IBFOA, were utilized to forecast the daily electricity load in Peninsular Malaysia for short-term analysis. The LSSVM model was trained using the RBF as the kernel function, while IBFOA was employed to optimize the parameters of LSSVM. The input from historical load data was separated into 5-day types in a week as follows:

- Day type: Monday
- Day type: Tuesday, Wednesday, Thursday (Tuesday–Thursday)
- Day type: Friday
- Day type: Saturday
- Day type: Sunday

Forecasts for Tuesday, Wednesday, and Thursday of each month were aligned due to their similar load curve patterns.

Figure 7a–e compared the forecast load demand from DNN, LSSVM, LSSVM-BFOA, and LSSVM-IBFOA models with the actual load demand for each day type in the testing dataset for four weeks. Considering 5-day types, each model generated one-day-ahead load profile forecasts for four consecutive weeks, from the third week of December 2021 to the second week of January 2022 (15 December 2021–14 January 2022) for short-term analysis. From the observation of actual load, the load demand fluctuates depending on the time of day, starting from modest levels in the early morning, rising as the day progresses, and slowing down as night approaches. Also, the load demand curve on weekends, especially Sundays, appears different compared to the weekday (Monday to Friday) load demand curve. The Sunday load profile exhibits a distinct pattern with a higher starting demand from 12:00 a.m., a gradual decrease until 8:00 a.m., and a subsequent rise until 7:00 p.m. The data separation highlights the importance of incorporating predefined day types in the forecasting model.

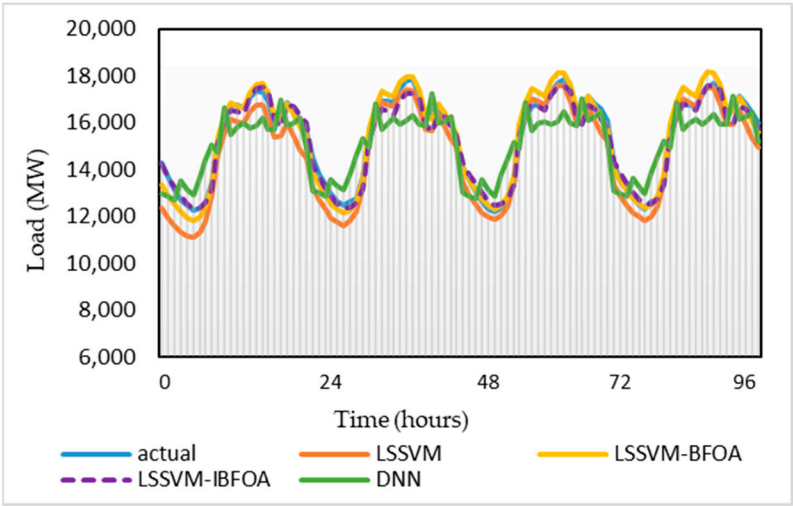

(**a**) Monday

Figure 7. *Cont.*

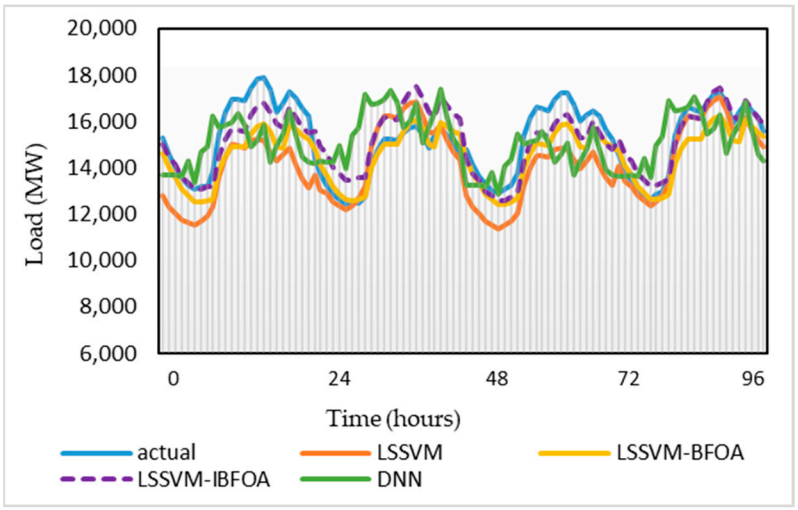

(**b**) Tuesday–Thursday

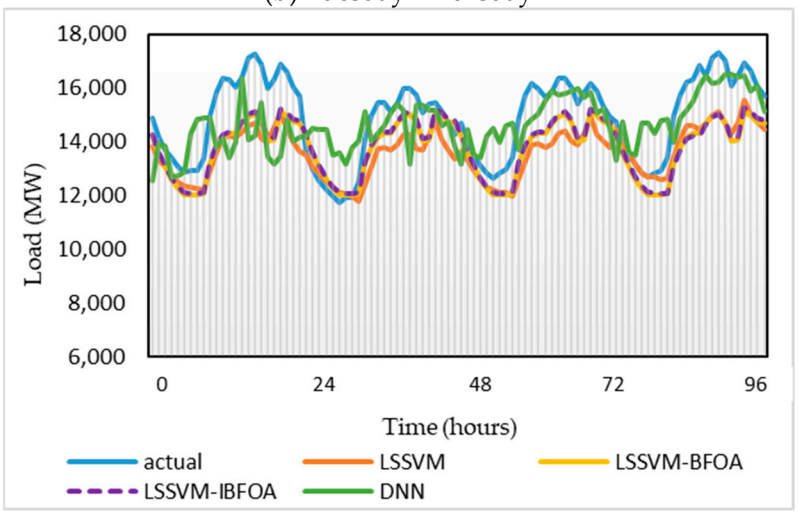

(**c**) Friday

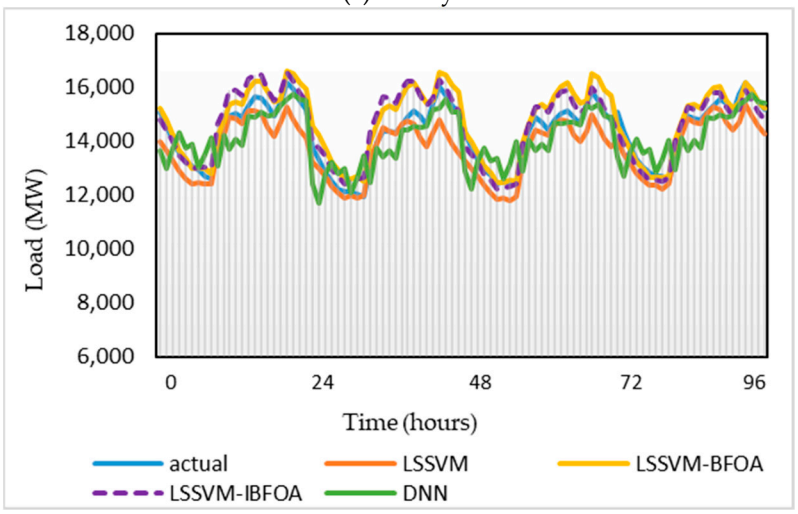

(**d**) Saturday

Figure 7. *Cont.*

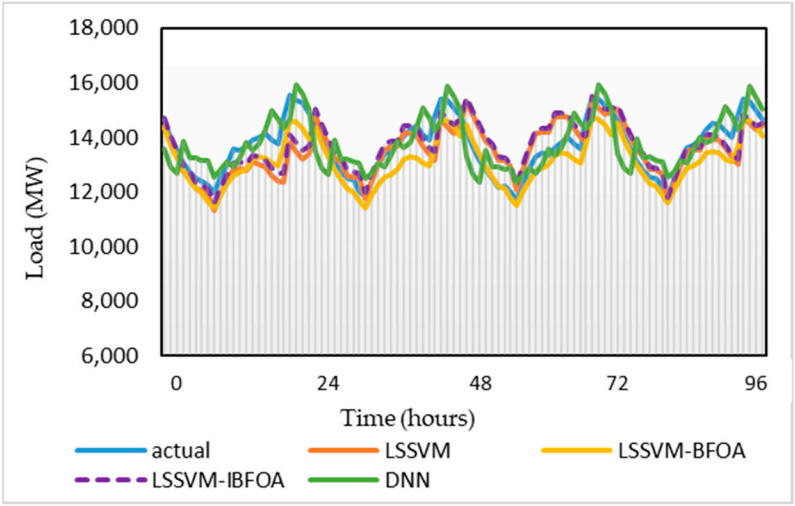

(**e**) Sunday

Figure 7. Visualization of forecasting result for the DNN, LSSVM, LSSVM-BFOA, and LSSVM-IBFOA for (**a**) Monday; (**b**) Tuesday–Thursday; (**c**) Friday; (**d**) Saturday, and (**e**) Sunday.

The simulations show that the forecasted load curve by the four models on Monday has the most similar pattern to the actual load curve as depicted in Figure 7a. An analysis of the average absolute differences reveals a clear advantage for the LSSVM-IBFOA model in consistently following the actual load profile across all four weeks. Particularly, LSSVM-IBFOA, LSSVM-BFOA, LSSVM, and DNN achieved the average absolute differences across the four weeks with values of 1.42%, 1.95%, 3.99%, and 6.04%, respectively. However, there is a gap between the forecasted load curve and the actual load curve at peak times of the day, especially on Friday and Tuesday–Thursday, which has the largest forecasting error value. The significant discrepancy between the forecasted and actual load, with all forecasting models underestimating demand is observed on the Friday load profile as shown in Figure 7c. Examining the average absolute differences across the four weeks' reveals that all models exhibited underestimation with the highest on the first week, with DNN (12.45%) showing the greatest deviation, LSSVM (10.27%), followed by LSSVM-BFOA (9.43%) and LSSVM-IBFOA (lowest—8.95%). For the weekend load profiles, while all forecasting models exhibited some level of underestimation, particularly during peak hours, the deviations were generally lower compared to other weekdays (Friday and Tuesday–Thursday).

Table 9 provides a detailed comparison of error metrics for the forecasting models evaluated on the 2021 testing dataset, categorized by day type (Monday through Sunday) for total of 96 sampling points. DNN outperforms LSSVM on Tuesday, Thursday, Friday, and Sunday, as indicated by lower error metrics. However, LSSVM exhibits superior performance on Monday and Saturday. These findings suggest that hybridizing LSSVM with IBFOA could potentially enhance its overall performance.

Through the analysis, LSSVM-IBFOA shows the consistently highest reductions in error metrics across all day types compared to DNN, LSSVM, and LSSVM-BFOA. Notably, across the five-day type, MAPE reductions obtained are 64.21%, 40.86%, 13.54%, 16.00%, and 7.24%, respectively, signifying significant improvements. Similarly, reductions were observed for MAE (62.45%, 42.70%, 14.35%, 17.35%, and 8.51%), RMSE and NRMSE (60.52%, 43.91%, 14.03%, 14.98%, and 17.30%), and MSE (84.41%, 68.54%, 26.10%, 27.72%, 31.62%). These reductions highlight the improved ability of LSSVM-IBFOA to minimize forecasting errors compared to the baseline LSSVM model.

Similarly, LSSVM-IBFOA outperformed LSSVM-BFOA with minimal reductions of MAPE (26.89%, 4.85%, 4.37%, 2.80%, and 0.19%), MAE (27.33%, 9.05%, 4.36%, 3.27%, and 2.00%), RMSE and NRMSE (25.10%, 3.99%, 3.42%, 0.17%, and 10.02%), and MSE (43.91%, 7.83%, 6.72%, 0.35%, 19.03%). In terms of R^2, the LSSVM-IBFOA achieves the highest value (0.9880) on Monday and the lowest (0.8901) on Friday. Conversely, LSSVM-BFOA and

LSSVM exhibit a wider range of R^2, with Mondays reaching 0.9824 and 0.9593, and Sundays dropping to 0.7405 and 0.4719, respectively. This observation suggests that LSSVM-IBFOA maintains a consistently high R^2 across weekdays, indicating a strong correlation between predicted and actual values.

Table 9. Forecasting accuracy of hybrid LSSVM-IBFOA and compared models.

Model	MAPE (%)	MAE (MW)	RMSE (MW)	MSE (MW)	NRMSE	R^2
Monday						
DNN	6.0479	906.6782	1020.2530	1,040,916.2167	0.0666	0.7344
LSSVM	4.0025	586.6865	710.5824	504,927.3971	0.0464	0.9593
LSSVM-BFOA	1.9592	303.1394	374.5812	140,311.0720	0.0244	0.9824
LSSVM-IBFOA	1.4324	220.2668	280.5340	78,699.33177	0.0183	0.9880
Tuesday–Thursday						
DNN	6.5912	964.7379	1231.8604	1,517,480.1165	0.0816	0.3582
LSSVM	8.2086	1270.5557	1536.8228	2,361,824.3854	0.1013	0.5614
LSSVM-BFOA	5.1020	809.2579	897.7997	806,044.3621	0.0591	0.8357
LSSVM-IBFOA	4.8542	735.9945	861.9280	742,919.9222	0.0568	0.9451
Friday						
DNN	7.8070	1144.208	1482.2793	2,197,151.8130	0.0996	0.1839
LSSVM	8.3786	1303.5522	1503.8283	2,261,499.7912	0.1010	0.8292
LSSVM-BFOA	7.5746	1167.3021	1338.5298	1,791,662.0492	0.0899	0.8834
LSSVM-IBFOA	7.2436	1116.3861	1292.7109	1671,101.5480	0.0868	0.8901
Saturday						
DNN	4.3742	611.1440	772.4642	596,700.8900	0.0540	0.5979
LSSVM	3.7320	543.9430	661.4871	437,565.1258	0.0462	0.8876
LSSVM-BFOA	3.2253	464.7921	563.3847	317,402.3313	0.0393	0.9295
LSSVM-IBFOA	3.1348	449.5594	562.3752	316,265.9746	0.0393	0.9606
Sunday						
DNN	4.2268	573.4755	659.2291	434,583.0080	0.0482	0.6144
LSSVM	4.4664	618.7235	789.2292	622,882.7987	0.0577	0.4719
LSSVM-BFOA	4.1507	577.6956	725.2978	526,056.9152	0.0530	0.7405
LSSVM-IBFOA	4.1427	566.0997	652.6199	425,912.8607	0.0477	0.9479
Average						
DNN	5.8094	840.0488	3669.8426	43,732,764.2466	0.2472	0.4978
LSSVM	5.7576	864.6922	1040.3900	1,237,739.8996	0.0705	0.7419
LSSVM-BFOA	4.4024	664.4374	779.9860	716,295.3460	0.0532	0.8743
LSSVM-IBFOA	4.1615	617.6613	730.0336	646,979.9275	0.0498	0.9464

While both LSSVM-IBFOA and LSSVM-BFOA demonstrate effectiveness compared to LSSVM and DNN, LSSVM-IBFOA outperforms LSSVM-BFOA on average. These observations on the testing dataset highlight the effectiveness of LSSVM-IBFOA in achieving superior overall forecasting accuracy. The optimization process introduced by the IBFOA algorithm empowers LSSVM to deliver forecasts with consistently lower errors and a strong positive correlation with actual values across different weekdays and weekends. These reductions highlight the effectiveness of LSSVM-IBFOA's optimization process in generalizing well to unseen data compared to LSSVM-BFOA.

Figure 8 summarizes the visualization results of accuracy measures from three models focusing on the important results. The error values of the models obtained demonstrate that Monday had the best performance with high accuracy compared to other day types. This result may be attributed to the relatively fewer public holidays in the historical load data occurring on Mondays compared to other day types throughout 2021. Consequently, a similar pattern of Monday was observed across all weeks and months of the year, pro-

ducing higher accuracy of load profile forecasting. The performance accuracy of models for other day types could be enhanced by incorporating specific public holiday data as additional features in the analysis.

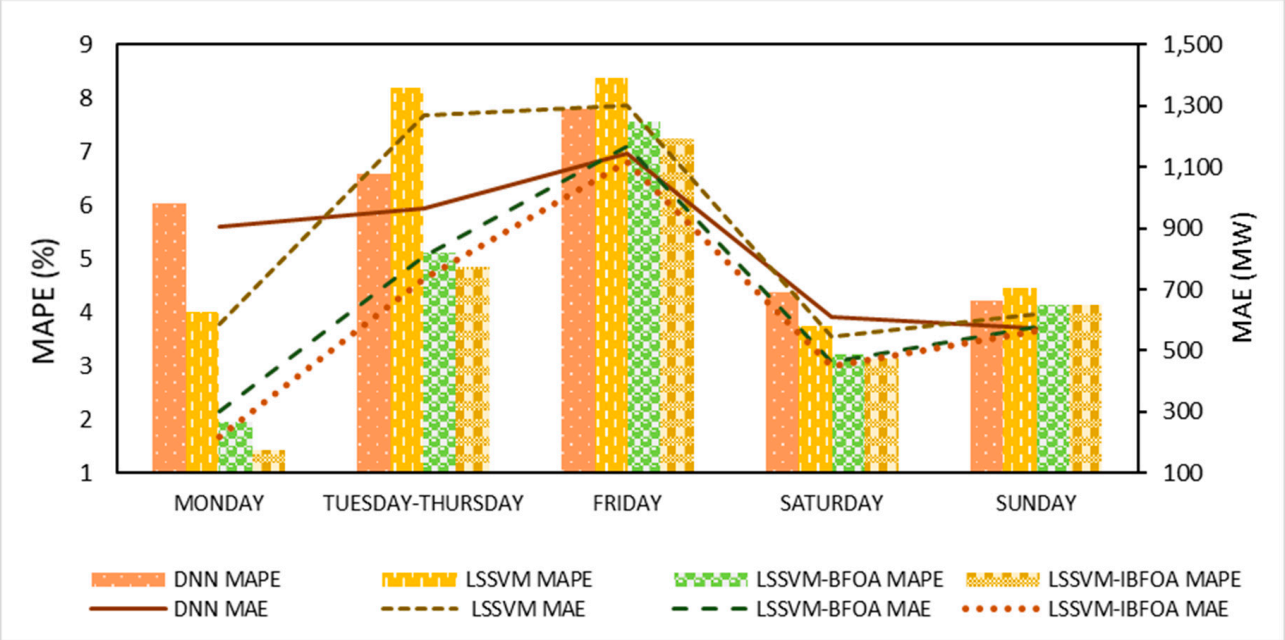

Figure 8. Illustrations of plots for MAPE and MAE.

From the above analysis, the electricity load forecasting result of using IBFOA to optimize the LSSVM model demonstrated better results than standard BFOA, stand-alone LSSVM, and DNN. Thus, the effectiveness of the proposed hybrid model is proved.

4.4. Algorithm Performance

Figure 9a–e depicts the convergence curve for IBFOA and BFOA, which is represented by the fitness value (MAPE) over the iteration. Table 10 represents the convergence time obtained for each day type, which shows that the IBFOA has a shorter convergence time than the BFOA. The IBFOA improves the convergence speed and accuracy of BFOA. SCA has a high speed due to its simple structure. At the same time, the reproduction and elimination dispersal processes give BFOA an advantage in accelerating the exploitation phase and preventing the algorithm from falling into local optima.

Table 10. Summary of the best convergence time for BFOA and IBFOA.

Day Type	Algorithm	Convergence Time (Minutes)
Monday	BFOA	44.6826
	IBFOA	38.1281
Tuesday–Thursday	BFOA	31.2697
	IBFOA	26.9290
Friday	BFOA	25.8514
	IBFOA	16.5285
Saturday	BFOA	35.5887
	IBFOA	21.7109
Sunday	BFOA	33.8185
	IBFOA	31.6932

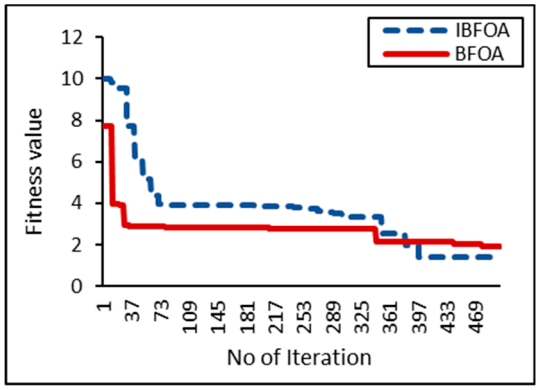

(**a**) Monday

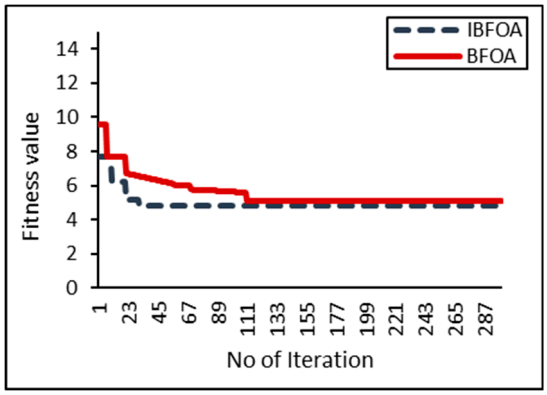

(**b**) Tuesday–Thursday

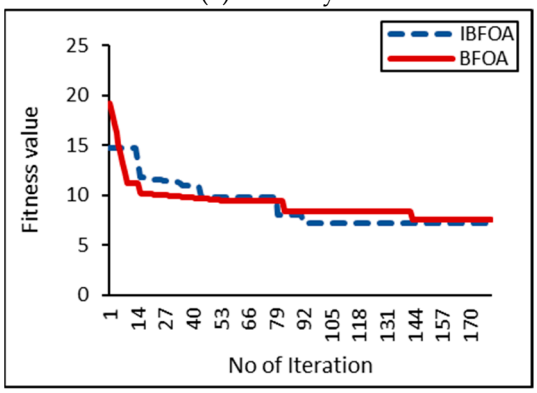

(**c**) Friday

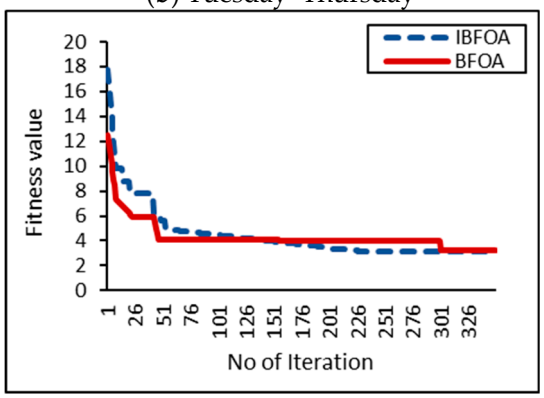

(**d**) Saturday

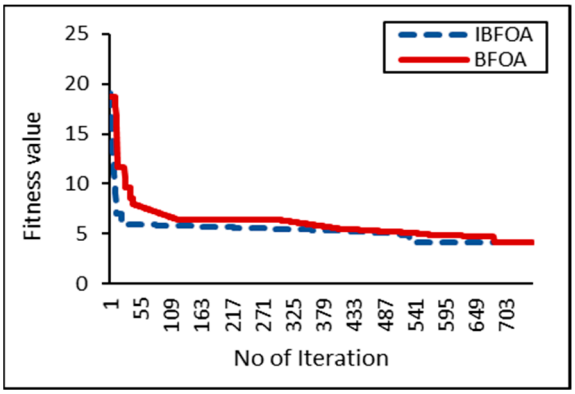

(**e**) Sunday

Figure 9. Convergence curve of BFOA and IBFOA for (**a**) Monday; (**b**) Tuesday–Thursday; (**c**) Friday; (**d**) Saturday; and (**e**) Sunday.

Therefore, the IBFOA has better performance in terms of convergence speed, accuracy, and local optima avoidance by synergizing the strengths of both algorithms. From the analysis, considering five-day types in a week, the IBFOA converges at 398th, 31st, 92nd, 231th, and 532th iterations, respectively. In contrast, the BFOA converges at the 477th, 111th, 143rd, 301st, and 682nd iterations, respectively.

5. Conclusions

Understanding future electricity demand patterns constitutes a critical factor in ensuring the stability and security of energy systems especially in Malaysia's power market. This information proves invaluable for government authorities as they make strategic decisions and plan a power system for the sustainable growth of a country. To forecast the

electric load accurately, in this paper, a hybrid method based on LSSVM optimized by IBFOA (LSSVM-IBFOA) for daily electricity load forecasting is proposed.

The Pearson correlation is utilized to analyze the correlation of present load with past load and weather. The past weather data incorporating temperature, humidity, and dew point are negligible since they show no until moderate correlation with the load. Thus, the historical load with a strong correlation is taken as the input to the LSSVM. While Pearson correlation analysis is useful for identifying linear relationships, it can be limited by its sensitivity to outliers and its inability to detect non-linear relationships. To address these shortcomings, advanced feature engineering techniques like Spearman rank correlation, random forest, and gradient boosting can be incorporated into the models to enhance feature selection accuracy in load forecasting.

For parameter optimization of LSSVM, an IBFOA is proposed to overcome the shortcomings of fixed constant value in chemotaxis from the original BFOA. Comparative analyses of algorithm performance demonstrated that IBFOA significantly enhances convergence accuracy and optimization performance, as evidenced by superior convergence curves and reduced convergence times. The proposed approach, LSSVM-IBFOA, is used to forecast the daily electricity load in peninsular Malaysia during the pandemic based on the historical load data in the year 2021, considering the five-day types in a week. The simulation result demonstrates that the hybrid of LSSVM-IBFOA outperforms the DNN, LSSVM, and LSSM-BFOA with the lowest value of MAPE, MAE, RMSE, MSE, and NRMSE as well as the biggest R^2 for all day types. On average, the values obtained from the day type were 4.1615%, 617.6613, 730.0336, 646,979.9275, 0.0498, and 0.9464, respectively. Additionally, detailed analyses across five-day types revealed that all models exhibited the highest accuracy on Mondays and the lowest on Fridays. Consequently, future research should focus on improving the performance of these models for other days of the week.

While this study focused on Malaysia, a country with a tropical climate influenced by monsoons, the proposed methodology offers potential for application in regions with four seasons. To enhance forecasting accuracy in such areas, seasonal variations should be considered, and meteorological parameters affecting load demand in each season should be identified through correlation analysis. For countries in Southeast Asia with similar climatic conditions, researchers can consider using the same meteorological parameters to identify the potential inputs to the model in the correlation analysis. Additionally, the IBFOA parameters can be adjusted accordingly to accommodate the specific characteristics of different datasets and regional variations, demonstrating the model's adaptability.

The recommendations for future directions are included but not limited to:

(a) Application for LSSVM-IBFOA for forecasting on a smaller load aggregation for residential and commercial buildings or considering specific electrical loads such as air-conditioning;
(b) Perform forecasting analyses using two approaches: one incorporating weather data as input features, and another relying solely on historical load data during normal periods;
(c) Inclusion of sensitivity analysis on the tuning parameters of the hybrid method;
(d) Adding more experiments for calculation of speed and resources of the forecasting model.

Author Contributions: F.A.Z.; methodology, writing—original draft preparation, software, M.F.S.; writing—review and editing, supervision, I.A.W.A.R.; software, methodology, validation, M.L.O.; writing—review and editing, H.M.; visualization and investigation. All authors have read and agreed to the published version of the manuscript.

Funding: The study is funding by Ministry of Higher Education (MOHE) of Malaysia through the Fundamental Research Grant Scheme (FRGS), No: (FRGS/1/2022/TK07/UTEM/02/53).

Data Availability Statement: The data presented in this study are available on request from the corresponding author due to restrictions on privacy.

Acknowledgments: The authors would like to thank Universiti Teknikal Malaysia Melaka (UTeM) for all the support given.

Conflicts of Interest: The authors declare no conflicts of interest. The funders had no role in the design of the study; in the collection, analyses, or interpretation of data; in the writing of the manuscript; or in the decision to publish the results.

Abbreviations

ANN	Artificial neural network
ARIMA	Auto-regressive integrated moving average
BFOA	Bacterial foraging optimization algorithm
CDD	Cooling degree days
CV-RMSE	Cross-validation root mean square error
DNN	Deep neural network
EMS	Energy management system
GDP	Gross domestic product
HDD	Heating degree days
IBFOA	Improved bacterial foraging optimization algorithm
LF	Load forecasting
LSSVM	Least square support vector machine
LSTM	Long short-term memory
LTLF	Long term load forecasting
MAE	Mean absolute error
MAPE	Mean absolute percentage error
MCO	Movement control order
ML	Machine learning
MSE	Mean square error
MTLF	Medium term load forecasting
NRMSE	Normalized root mean square error
PCC	Pearson's correlation coefficient
R^2	Determination coefficient
RE	Renewable energy
RMSE	Root mean square error
SARIMA	Seasonal auto-regressive integrated moving average
STLF	Short-term load forecasting
SVM	Support vector machine
VSTLF	Very short-term load forecasting

References

1. Zulkifli, Z. Malaysia Country Report. In Proceedings of the 17th Asia Construct Conference, Seoul, Republic of Korea, 17 December 2021; pp. 170–190.
2. IRENA. *Malaysia Energy Transition Outlook*; International Renewable Energy Agency: Abu Dhabi, United Arab Emirates, 2023; ISBN 978-92-9260-357-1.
3. Aswanuwath, L.; Pannakkong, W.; Buddhakulsomsiri, J.; Karnjana, J. An Improved Hybrid Approach for Daily Electricity Peak Demand Forecasting during Disrupted Situations: A Case Study of COVID-19 Impact in Thailand. *Energies* **2023**, *17*, 78. [CrossRef]
4. Mir, A.A.; Alghassab, M.; Ullah, K.; Khan, Z.A.; Lu, Y.; Imran, M. A review of electricity demand forecasting in low and middle income countries: The demand determinants and horizons. *Sustainability* **2020**, *12*, 5931. [CrossRef]
5. Koukaras, P.; Bezas, N.; Gkaidatzis, P.; Ioannidis, D.; Tzovaras, D.; Tjortjis, C. Introducing a novel approach in one-step ahead energy load forecasting. *Sustain. Comput. Inform. Syst.* **2021**, *32*, 100616. [CrossRef]
6. Moon, J.; Jung, S.; Rew, J.; Rho, S.; Hwang, E. Combination of short-term load forecasting models based on a stacking ensemble approach. *Energy Build.* **2020**, *216*, 109921. [CrossRef]
7. Islam, B.U.; Rasheed, M.; Ahmed, S.F. Review of Short-Term Load Forecasting for Smart Grids Using Deep Neural Networks and Metaheuristic Methods. *Math. Probl. Eng.* **2022**, *2022*, 4049685. [CrossRef]
8. Nti, I.K.; Teimeh, M.; Nyarko-Boateng, O.; Adekoya, A.F. Electricity load forecasting: A systematic review. *J. Electr. Syst. Inf. Technol.* **2020**, *7*, 13. [CrossRef]
9. Hammad, M.A.; Jereb, B.; Rosi, B.; Dragan, D. Methods and Models for Electric Load Forecasting: A Comprehensive Review. *Logist. Sustain. Transp.* **2020**, *11*, 51–76. [CrossRef]

10. Han, Y.; Xiong, H.; Wei, D. Short-term load forecasting of BP network based on bacterial foraging optimization. *IOP Conf. Ser. Mater. Sci. Eng.* **2019**, *569*, 052082. [CrossRef]
11. Zhou, Z.; Wu, G.; Zhang, X. Short-term Load Forecasting Model Based on IBFO-BILSTM. *IOP Conf. Ser. Earth Environ. Sci.* **2020**, *440*, 032134. [CrossRef]
12. Zhang, Y.; Wu, L.; Wang, S. Bacterial foraging optimization based neural network for short-term load forecasting. *J. Comput. Inf. Syst.* **2010**, *6*, 2099–2105.
13. Pelekis, S.; Seisopoulos, I.-K.; Spiliotis, E.; Pountridis, T.; Karakolis, E.; Mouzakitis, S.; Askounis, D. A comparative assessment of deep learning models for day-ahead load forecasting: Investigating key accuracy drivers. *Sustain. Energy Grids Netw.* **2023**, *36*, 101171. [CrossRef]
14. Luo, H.; Zhang, H.; Wang, J. Ensemble power load forecasting based on competitive-inhibition selection strategy and deep learning. *Sustain. Energy Technol. Assess.* **2022**, *51*, 101940. [CrossRef]
15. Tarmanini, C.; Sarma, N.; Gezegin, C.; Ozgonenel, O. Short term load forecasting based on ARIMA and ANN approaches. *Energy Rep.* **2023**, *9*, 550–557. [CrossRef]
16. Amjady, N.; Keynia, F. A new neural network approach to short term load forecasting of electrical power systems. *Energies* **2011**, *4*, 488–503. [CrossRef]
17. Jawad, M.; Nadeem, M.S.A.; Shim, S.O.; Khan, I.R.; Shaheen, A.; Habib, N.; Hussain, L.; Aziz, W. Machine Learning Based Cost Effective Electricity Load Forecasting Model Using Correlated Meteorological Parameters. *IEEE Access* **2020**, *8*, 146847–146864. [CrossRef]
18. Stamatellos, G.-T.L.F.; Stamatelos, T. Short-Term Load Forecasting of the Greek Electricity System. *Appl. Sci.* **2023**, *13*, 2719. [CrossRef]
19. Ahmed, T.; Vu, D.H.; Muttaqi, K.M.; Agalgaonkar, A.P. Load forecasting under changing climatic conditions for the city of Sydney, Australia. *Energy* **2018**, *142*, 911–919. [CrossRef]
20. Ahmad, T.; Chen, H.; Shair, J.; Xu, C. Deployment of data-mining short and medium-term horizon cooling load forecasting models for building energy optimization and management. *Int. J. Refrig.* **2019**, *98*, 399–409. [CrossRef]
21. Wang, Y.; Chen, J.; Chen, X.; Zeng, X.; Kong, Y.; Sun, S.; Guo, Y.; Liu, Y. Short-term load forecasting for industrial customers based on TCN-LightGBM. *IEEE Trans. Power Syst.* **2021**, *36*, 1984–1997. [CrossRef]
22. Yang, A.; Li, W.; Yang, X. Short-term electricity load forecasting based on feature selection and Least Squares Support Vector Machines. *Knowl.-Based Syst.* **2019**, *163*, 159–173. [CrossRef]
23. Li, S.; Kong, X.; Yue, L.; Liu, C.; Khan, M.A.; Yang, Z.; Zhang, H. Short-term electrical load forecasting using hybrid model of manta ray foraging optimization and support vector regression. *J. Clean. Prod.* **2023**, *388*, 135856. [CrossRef]
24. Chaianong, A.; Winzer, C.; Gellrich, M. Impacts of traffic data on short-term residential load forecasting before and during the COVID-19 pandemic. *Energy Strateg. Rev.* **2022**, *43*, 100895. [CrossRef]
25. Yang, L.; Yang, S.; Li, S.; Zhang, R.; Liu, F.; Jiao, L. Coupled compressed sensing inspired sparse spatial-spectral LSSVM for hyperspectral image classification. *Knowl.-Based Syst.* **2015**, *79*, 80–89. [CrossRef]
26. Ge, Q.; Guo, C.; Jiang, H.; Lu, Z.; Yao, G.; Zhang, J.; Hua, Q. Industrial Power Load Forecasting Method Based on Reinforcement Learning and PSO-LSSVM. *IEEE Trans. Cybern.* **2022**, *52*, 1112–1124. [CrossRef] [PubMed]
27. Wang, G.; Wang, X.; Wang, Z.; Ma, C.; Song, Z. A VMD-CISSA-LSSVM Based Electricity Load Forecasting Model. *Mathematics* **2022**, *10*, 28. [CrossRef]
28. Zhang, S.; Zhang, N.; Zhang, Z.; Chen, Y. Electric Power Load Forecasting Method Based on a Support Vector Machine Optimized by the Improved Seagull Optimization Algorithm. *Energies* **2022**, *15*, 9197. [CrossRef]
29. Khan, B.; Redae, K.; Gidey, E.; Mahela, O.P.; Taha, I.B.M.; Hussien, M.G. Optimal integration of DSTATCOM using improved bacterial search algorithm for distribution network optimization. *Alex. Eng. J.* **2022**, *61*, 5539–5555. [CrossRef]
30. Awad, H.; Hafez, A. Optimal operation of under-frequency load shedding relays by hybrid optimization of particle swarm and bacterial foraging algorithms. *Alex. Eng. J.* **2022**, *61*, 763–774. [CrossRef]
31. Nguyen, H.M.V.; Phung, T.T.; Le, T.N.; Nguyen, N.A.; Nguyen, Q.T.; Nguyen, P.N. Using an improved Neural Network with Bacterial Foraging Optimization algorithm for Load Shedding. In Proceedings of the 2023 International Conference on System Science and Engineering (ICSSE), Ho Chi Minh, Vietnam, 27–28 July 2023; pp. 281–286. [CrossRef]
32. Tounsi Fokui, W.S.; Saulo, M.J.; Ngoo, L. Optimal Placement of Electric Vehicle Charging Stations in a Distribution Network with Randomly Distributed Rooftop Photovoltaic Systems. *IEEE Access* **2021**, *9*, 132397–132411. [CrossRef]
33. Panwar, A.; Sharma, G.; Nasiruddin, I.; Bansal, R.C. Frequency stabilization of hydro–hydro power system using hybrid bacteria foraging PSO with UPFC and HAE. *Electr. Power Syst. Res.* **2018**, *161*, 74–85. [CrossRef]
34. Kumar, R.; Diwania, S.; Singh, R.; Ashfaq, H.; Khetrapal, P.; Singh, S. An intelligent Hybrid Wind–PV farm as a static compensator for overall stability and control of multimachine power system. *ISA Trans.* **2022**, *123*, 286–302. [CrossRef] [PubMed]
35. Zadehbagheri, M.; Sutikno, T.; Kiani, M.J.; Yousefi, M. Designing a power system stabilizer using a hybrid algorithm by genetics and bacteria for the multi-machine power system. *Bull. Electr. Eng. Inform.* **2023**, *12*, 1318–1331. [CrossRef]
36. Zhang, Y.; Lv, Y.; Zhou, Y. Research on Economic Optimal Dispatching of Microgrid Based on an Improved Bacteria Foraging Optimization. *Biomimetics* **2023**, *8*, 150. [CrossRef] [PubMed]
37. de Moraes, C.H.V.; Boas, J.L.d.V.; Lambert-Torres, G.; de Andrade, G.C.C.; Costa, C.I.d.A. Intelligent Power Distribution Restoration Based on a Multi-Objective Bacterial Foraging Optimization Algorithm. *Energies* **2022**, *15*, 1445. [CrossRef]

38. Chen, Y.; Xiao, C.; Yang, S.; Yang, Y.; Wang, W. Research on long term power load grey combination forecasting based on fuzzy support vector machine. *Comput. Electr. Eng.* **2024**, *116*, 109205. [CrossRef]
39. Zhou, M.; Yu, J.; Wang, M.; Quan, W.; Bian, C. Research on the combined forecasting model of cooling load based on IVMD-WOA-LSSVM. *Energy Build.* **2024**, *317*, 114339. [CrossRef]
40. Bakare, M.S.; Abdulkarim, A.; Shuaibu, A.N.; Muhamad, M.M. A hybrid long-term industrial electrical load forecasting model using optimized ANFIS with gene expression programming. *Energy Rep.* **2024**, *11*, 5831–5844. [CrossRef]
41. Lotfipoor, A.; Patidar, S.; Jenkins, D.P. Deep neural network with empirical mode decomposition and Bayesian optimisation for residential load forecasting. *Expert Syst. Appl.* **2024**, *237*, 121355. [CrossRef]
42. Jahani, A.; Zare, K.; Mohammad Khanli, L. Short-term load forecasting for microgrid energy management system using hybrid SPM-LSTM. *Sustain. Cities Soc.* **2023**, *98*, 104775. [CrossRef]
43. Zhao, X.; Shen, B.; Lin, L.; Liu, D.; Yan, M.; Li, G. Residential Electricity Load Forecasting Based on Fuzzy Cluster Analysis and LSSVM with Optimization by the Fireworks Algorithm. *Sustainability* **2022**, *14*, 1312. [CrossRef]
44. Li, J.; Lei, Y.; Yang, S. Mid-long term load forecasting model based on support vector machine optimized by improved sparrow search algorithm. *Energy Rep.* **2022**, *8*, 491–497. [CrossRef]
45. Jiang, Y.; Huang, Q.; Zhang, K.; Lin, Z.; Zhang, T.; Hu, X.; Liu, S.; Jiang, C.; Yang, L.; Lin, Z. Medium-long term load forecasting method considering industry correlation for power management. *Energy Rep.* **2021**, *7*, 1231–1238. [CrossRef]
46. Zhi, X.; Yuexin, S.; Jin, M.; Lujie, Z.; Zijian, D. Research on the Pearson correlation coefficient evaluation method of analog signal in the process of unit peak load regulation. In Proceedings of the 2017 13th IEEE International Conference on Electronic Measurement & Instruments (ICEMI), Yangzhou, China, 20–22 October 2017; pp. 522–527. [CrossRef]
47. Sukarti, S.; Sulaima, M.F.; Kadir, A.F.A.; Shamsor, M.H.; Yao, S.W. Advancing industrial building energy measurement and verification (M&V) with deep learning: Evaluating data size and feature selection impact. *Energy Build.* **2024**, *319*, 114457. [CrossRef]
48. Suykens, J.A.K.; Vandewalle, J. Least Squares Support Vector Machine Classifiers. *Neural Process. Lett.* **1999**, *9*, 293–300. [CrossRef]
49. Gao, K.; Xu, X.; Jiao, S. Prediction and visualization analysis of drilling energy consumption based on mechanism and data hybrid drive. *Energy* **2022**, *261*, 125227. [CrossRef]
50. Yuan, X.; Chen, C.; Yuan, Y.; Huang, Y.; Tan, Q. Short-term wind power prediction based on LSSVM-GSA model. *Energy Convers. Manag.* **2015**, *101*, 393–401. [CrossRef]
51. Passino, K.M. Biomimicry of Bacterial Foraging for Distributed Optimization and Control. *IEEE Control Syst.* **2002**, *22*, 52–67. [CrossRef]
52. Zhang, Y.; Lv, Y. Research on electrical load distribution using an improved bacterial foraging algorithm. *Front. Energy Res.* **2023**, *11*, 1103038. [CrossRef]
53. Lee, C.Y.; Lee, Z.J.; Huang, J.Q.; Ye, F.L.; Yao, J.; Ning, Z.Y.; Meen, T.H. Hybrid algorithm based on simulated annealing and bacterial foraging optimization for mining imbalanced data. *Sens. Mater.* **2021**, *33*, 1297–1312. [CrossRef]
54. Sharma, A. Adaptive bacterial foraging optimization based task scheduling in cloud computing. *J. Green Eng.* **2020**, *10*, 10189–10202.
55. Mohammad, S.; Mat Jusof, M.F.; Mhd Rizal, N.A.; Abd Razak, A.A.; Nasir, A.N.K.; Ismail, R.M.T.R.; Ahmad, M.A. Sine based Bacterial Foraging Algorithm for a Dynamic Modelling of a Twin Rotor System. In Proceedings of the 2019 19th International Conference on Control, Automation and Systems (ICCAS), Jeju, Republic of Korea, 15–18 October 2019; pp. 131–136. [CrossRef]
56. Ahmad, N.; Ghadi, Y.; Adnan, M.; Ali, M. Load Forecasting Techniques for Power System: Research Challenges and Survey. *IEEE Access* **2022**, *10*, 71054–71090. [CrossRef]
57. Hong, T.; Fan, S. Probabilistic electric load forecasting: A tutorial review. *Int. J. Forecast.* **2016**, *32*, 914–938. [CrossRef]
58. Vivas, E.; Allende-Cid, H.; Salas, R. A systematic review of statistical and machine learning methods for electrical power forecasting with reported mape score. *Entropy* **2020**, *22*, 1412. [CrossRef] [PubMed]
59. Wang, J.; Du, P.; Lu, H.; Yang, W.; Niu, T. An improved grey model optimized by multi-objective ant lion optimization algorithm for annual electricity consumption forecasting. *Appl. Soft Comput. J.* **2018**, *72*, 321–337. [CrossRef]
60. Zhao, H.; Guo, S. An optimized grey model for annual power load forecasting. *Energy* **2016**, *107*, 272–286. [CrossRef]
61. Sekhar, C.; Dahiya, R. Robust framework based on hybrid deep learning approach for short term load forecasting of building electricity demand. *Energy* **2023**, *268*, 126660. [CrossRef]
62. Moradzadeh, A.; Zakeri, S.; Shoaran, M.; Mohammadi-Ivatloo, B.; Mohammadi, F. Short-term load forecasting of microgrid via hybrid support vector regression and long short-term memory algorithms. *Sustainability* **2020**, *12*, 7076. [CrossRef]
63. Fan, G.F.; Zhang, L.Z.; Yu, M.; Hong, W.C.; Dong, S.Q. Applications of random forest in multivariable response surface for short-term load forecasting. *Int. J. Electr. Power Energy Syst.* **2022**, *139*, 108073. [CrossRef]
64. Tsalikidis, N.; Mystakidis, A.; Tjortjis, C.; Koukaras, P.; Ioannidis, D. Energy load forecasting: One-step ahead hybrid model utilizing ensembling. *Computing* **2023**, *106*, 241–273. [CrossRef]
65. Groß, A.; Lenders, A.; Schwenker, F.; Braun, D.A.; Fischer, D. Comparison of short-term electrical load forecasting methods for different building types. *Energy Inform.* **2021**, *4* (Suppl. S3), 13. [CrossRef]
66. Kök, A.; Yükseltan, E.; Hekimoğlu, M.; Aktunc, E.A.; Yücekaya, A.; Bilge, A. Forecasting Hourly Electricity Demand Under COVID-19 Restrictions. *Int. J. Energy Econ. Policy* **2022**, *12*, 73–85. [CrossRef]

67. Park, R.J.; Song, K.B.; Kwon, B.S. Short-term load forecasting algorithm using a similar day selection method based on reinforcement learning. *Energies* **2020**, *13*, 2640. [CrossRef]
68. Xie, J.; Zhong, Y.; Xiao, T.; Wang, Z.; Zhang, J.; Wang, T.; Schuller, B.W. A multi-information fusion model for short term load forecasting of an architectural complex considering spatio-temporal characteristics. *Energy Build.* **2022**, *277*, 112566. [CrossRef]
69. Jiang, Z.; Zhang, L.; Ji, T. NSDAR: A neural network-based model for similar day screening and electric load forecasting. *Appl. Energy* **2023**, *349*, 121647. [CrossRef]
70. Son, J.; Cha, J.; Kim, H.; Wi, Y.M. Day-Ahead Short-Term Load Forecasting for Holidays Based on Modification of Similar Days' Load Profiles. *IEEE Access* **2022**, *10*, 17864–17880. [CrossRef]
71. Madrid, E.A.; Antonio, N. Short-term electricity load forecasting with machine learning. *Information* **2021**, *12*, 50. [CrossRef]
72. Mandal, P.; Senjyu, T.; Urasaki, N.; Funabashi, T. A neural network based several-hour-ahead electric load forecasting using similar days approach. *Int. J. Electr. Power Energy Syst.* **2006**, *28*, 367–373. [CrossRef]
73. Barman, M.; Dev Choudhury, N.B. Season specific approach for short-term load forecasting based on hybrid FA-SVM and similarity concept. *Energy* **2019**, *174*, 886–896. [CrossRef]
74. Lee, G.C. Regression-Based Methods for Daily Peak Load Forecasting in South Korea. *Sustainability* **2022**, *14*, 3984. [CrossRef]
75. Pinheiro, M.G.; Madeira, S.C.; Francisco, A.P. Short-term electricity load forecasting—A systematic approach from system level to secondary substations. *Appl. Energy* **2023**, *332*, 120493. [CrossRef]
76. Erişen, E.; Iyigun, C.; Tanrısever, F. Short-term electricity load forecasting with special days: An analysis on parametric and non-parametric methods. *Ann. Oper. Res.* **2017**, 1–34. [CrossRef]